Calculation of the two-loop heavy-flavor contribution to Bhabha scattering

Bonciani, R ; Ferroglia, A ; Penin, A A

Abstract: We describe in detail the calculation of the two-loop corrections to the QED Bhabha scattering cross section due to the vacuum polarization by heavy fermions. Our approach eliminates one mass scale from the most challenging part of the calculation and allows us to obtain the corrections in a closed analytical form. The result is valid for arbitrary values of the heavy fermion mass and the Mandelstam invariants, as long as s, t, u » me2.

DOI: https://doi.org/10.1088/1126-6708/2008/02/080

ALBERTA-THY-24-07
IFIC/07-77
ZU-TH 31/07

Calculation of the Two-Loop Heavy-Flavor Contribution to Bhabha Scattering

R. Bonciani [a,*], A. Ferroglia [b,†], and A.A. Penin [c,d,‡]

[a] *Departamento de Física Teòrica, IFIC, CSIC – Universidad de Valencia, E-46071 Valencia, Spain*

[b] *Institut für Theoretische Physik, Universität Zürich, CH-8057 Zurich, Switzerland*

[c] *Department of Physics, University Of Alberta, Edmonton, AB T6G 2J1, Canada*

[d] *Institute for Nuclear Research of Russian Academy of Sciences, 117312 Moscow, Russia*

Abstract

We describe in detail the calculation of the two-loop corrections to the QED Bhabha scattering cross section due to the vacuum polarization by heavy fermions. Our approach eliminates one mass scale from the most challenging part of the calculation and allows us to obtain the corrections in a closed analytical form. The result is valid for arbitrary values of the heavy fermion mass and the Mandelstam invariants, as long as $s, t, u \gg m_e^2$.

PACS numbers: 11.15.Bt, 12.20.Ds

*Email: Roberto.Bonciani@ific.uv.es
†Email: Andrea.Ferroglia@physik.unizh.ch
‡Email: apenin@phys.ualberta.ca

1 Introduction

High energy electron-positron or *Bhabha* scattering [1] is among the most important and carefully studied processes in particle physics. It provides a very efficient tool for luminosity determination at electron-positron colliders and thus mediates the process of extracting physical information from the raw experimental data [2]. The small-angle Bhabha scattering is particularly effective as a luminosity monitor at high-energy colliders.[4] The large-angle Bhabha scattering is used to measure the luminosity at colliders operating at the center-of-mass energy, $\sqrt{s}$, of a few GeV, such as BABAR/PEP-II, BELLE/KEKB, BES/BEPC, KLOE/DAΦNE, and CMD, SND/VEPP-2M [5].[5] Moreover, it will be also used to disentangle the luminosity spectrum at the ILC [6,7]. Bhabha scattering involves stable charged leptons both in the initial and the final states and, therefore, it can be measured experimentally with very high precision. At LEP, the experimental error in the luminosity measurement has been reduced to 0.4 permille [8] and it is expected to be even smaller at the ILC: the goal of the TESLA forward calorimeter collaboration is to reach the experimental accuracy of 0.1 permille in the first year of run [9]. Finally, at the low-energy accelerators DAΦNE and VEPP-2M the cross section of the large-angle scattering is measured with the accuracy of about 1 permille [10,11]. In the phenomenologically most interesting cases of low energy or small angle scattering, the Bhabha cross section is QED dominated, with the electroweak and hadronic effects being strongly suppressed. Therefore, it can be reliably computed in perturbative QED, with the accuracy limited only by uncalculated high order corrections. These properties make in such a way that Bhabha scattering is an ideal "standard candle" for electron-positron colliders.

Realistic simulations of the Bhabha events, which take into account the detector geometry and experimental cuts, are performed by means of sophisticated Monte Carlo generators, such as BHLUMI [12], BABAYAGA [13], BHAGENF [14], BHWIDE [15] and MCGPJ [16]. To match the experimental needs, the two-loop QED corrections must be included into the theoretical analysis and incorporated into the event generators. Since the theoretical accuracy directly affects the luminosity determination and may jeopardize the high-precision physics program at electron-positron colliders, remarkable efforts were devoted to the study of the radiative corrections. The one-loop corrections have been known in the full electroweak theory for a long time [17]. The two-loop electroweak corrections are still elusive. However, recently the calculation of the two-loop QED corrections was completed. These corrections can be divided into three main categories: (i) the pure photonic corrections, (ii) the corrections involving the electron vacuum polarization, *i.e.* with at least one closed electron loop, and (iii) the corrections involving the vacuum polarization by heavy flavors (leptons or quarks). The first results for the photonic corrections were obtained in the limit of small scattering angles [18,19,20,21], in the massless electron approximation [22], and for the terms enhanced by powers of the large logarithm $\ln(s/m_e^2)$ [23]. Finally, the photonic corrections to the differential cross section were obtained in [24] in the leading order of the small electron mass expansion through the *infrared matching* to the massless approximation. This result is sufficient for all phenomenological applications at present and future colliders [25] and was recently confirmed within a slightly

[4] At LEP, the luminometers were located at an angle between 1.4° and 2.9°. At the future International Linear Collider (ILC), they will be placed between 0.7° and 2.3° [3].

[5] For example, in KLOE experiment the luminosity measurement is based on the events with scattering angles between 55° and 125° [4].

different framework [26] (see also [27]).[6] The corrections involving a closed electron loop were obtained in [34,35,36] by direct diagrammatic calculation, retaining the full dependence on m_e. The calculation was performed by using the Laporta algorithm [37] for the reduction of the Feynman diagrams to the master integrals (MIs) [38], which were subsequently evaluated [29,30,31,32,33] by means of the differential equation method [39]. The result was obtained in analytical form in terms of harmonic polylogarithms [40,41,42,43]. The corrections due to the vacuum polarization by heavy fermion of mass $m_f \gg m_e$ were first evaluated in the limit $m_f^2 \ll s,t,u$ by two different methods [26,44]. The calculation of [26] is based on the expansion in the electron mass within the effective theory approach, while the calculation of [44] is diagrammatic and based on the reduction to the MIs evaluated in the asymptotic regime [45]. The condition $m_f^2 \ll s,t,u$, however, does not hold for τ-lepton, c- and b-quarks in the practically interesting energy range of about a few GeV, as well as for the top quark at typical ILC energies 500 GeV $\lesssim \sqrt{s} \lesssim$ 1000 GeV. In a recent letter [46] we announced the result for the two-loop heavy-flavor contribution which is valid for any ratio of the heavy fermion mass to the Mandelstam invariants, provided $s,t,u \gg m_e^2$. The calculation was performed in the small electron mass limit. We used the general theory of infrared and collinear divergencies to separate the singular dependence of the corrections on the vanishing electron mass. The most difficult part of the calculation was then carried out with a strictly massless electron. This critically reduced the complexity of the problem and made it solvable by the method of [34,35,36].[7]

In this paper we provide a detailed account of our calculation [46] and we present the complete analytical result for the correction to the Bhabha cross section. The paper is organized as follows. In Section 2 we introduce our notations and conventions. In Section 3 we discuss the infrared and collinear structure of the corrections and outline the strategy of the calculation. In Section 4 we describe the calculation of two previously unknown four-point two-loop master integrals. In Section 5 we present the analytical result for the correction to the cross section. The numerical analysis is given in Section 6. Section 7 contains our conclusions. Some technical aspects of the calculation including the auxiliary functions, generalized harmonic polylogarithms (GHPLs), and the asymptotic behavior of the corrections are discussed in the appendices.

2 Notation and Conventions

In this Section we briefly summarize our notation and conventions which follow [35,36]. We consider the photon mediated process

$$e^-(p_1) + e^+(p_2) \to e^-(p_3) + e^+(p_4)\,, \tag{1}$$

where $p_i^2 = -m_e^2$. In the following, we will neglect the electron mass, which is much smaller than any of the other mass scales involved in the problem. m_e will be set consistently to zero everywhere, except where it acts as a regulator for the collinear singularities. The kinematics

[6] The full dependence of the pure photonic corrections on the electron mass m_e is not known at the moment. The corresponding calculation involves the two-loop box diagrams with three scales: s, t and m_e, which are not yet available, though many relevant results have been already obtained [28,29,30,31,32,33].

[7] When this work was in preparation a numerical result for the two-loop heavy-flavor contribution was obtained by means of the dispersion relation approach [47].

of the process is described in terms of the Mandelstam invariants s, t and u:

$$s = -P^2 \equiv -(p_1+p_2)^2 = 4E^2\,, \tag{2}$$

$$t = -Q^2 \equiv -(p_1-p_3)^2 = -4E^2\sin^2\frac{\theta}{2}\,, \tag{3}$$

$$u = -R^2 \equiv -(p_1-p_4)^2 = -4E^2\cos^2\frac{\theta}{2}\,, \tag{4}$$

where $s+t+u=0$, E is the particle energy in the center-of-mass frame, and θ is the scattering angle. The Bhabha scattering differential cross section is given by a series in the fine-structure constant α:

$$\frac{d\sigma}{d\Omega} = \frac{d\sigma_0}{d\Omega} + \left(\frac{\alpha}{\pi}\right)\frac{d\sigma_1}{d\Omega} + \left(\frac{\alpha}{\pi}\right)^2\frac{d\sigma_2}{d\Omega} + \mathcal{O}\left(\alpha^3\right)\,, \tag{5}$$

where

$$\frac{d\sigma_0}{d\Omega} = \frac{\alpha^2}{s}\left[\frac{1}{s^2}\left(st+\frac{s^2}{2}+t^2\right)+\frac{1}{t^2}\left(st+\frac{t^2}{2}+s^2\right)+\frac{1}{st}(s+t)^2\right]+\mathcal{O}(m_e^2/s) \tag{6}$$

is the Born cross section. In this paper, we consider only the radiative corrections $d\sigma_i/d\Omega$ that involve the vacuum polarization by heavy fermions. The first order correction to the cross section comes from the interference of the diagrams (a) and (b) in Fig. 1 with the Born amplitude and it reads

$$\begin{aligned}\frac{d\sigma_1}{d\Omega} = {} & \frac{\alpha^2}{s}Q_f^2N_c\left[\frac{1}{s^2}\left(st+\frac{s^2}{2}+t^2\right)2\mathrm{Re}\Pi_0^{(1l,0)}(s)+\frac{1}{t^2}\left(st+\frac{t^2}{2}+s^2\right)2\Pi_0^{(1l,0)}(t)\right.\\ & \left.+\frac{1}{st}(s+t)^2\left(\mathrm{Re}\Pi_0^{(1l,0)}(s)+\Pi_0^{(1l,0)}(t)\right)\right]+\mathcal{O}(m_e^2/s)\,.\end{aligned} \tag{7}$$

The expression of the one-loop vacuum polarization functions $\Pi_0^{(1l,0)}$ is given in Appendix B; Q_f is the electric charge of the heavy fermion, N_c (number of colors) is equal to 1 for leptons and 3 for quarks, and we adopt the on-shell scheme for the renormalization of α and of the fermion mass. Note that Eq. (7) is infrared finite and has a regular behavior in the small electron mass limit.

3 Structure of the Second-Order Corrections and Calculation Method

The two-loop virtual corrections are infrared divergent. These *soft* divergencies are canceled in the inclusive cross section when one adds the photonic bremsstrahlung [48]. We regulate all the soft divergencies by dimensional regularization in D space-time dimensions. The standard approach to deal with the bremsstrahlung is to split it into a soft part, which accounts for the emission of the photons with the energy below a given cut-off $\omega \ll m_e$, and a hard part corresponding to the emission of the photons with the energy larger than ω. The infrared finite hard part is then computed numerically using Monte-Carlo methods with physical cuts dictated by the experimental setup. At the same time, the soft part is computed analytically and combined with the virtual corrections ensuring the cancellation of the soft divergencies in

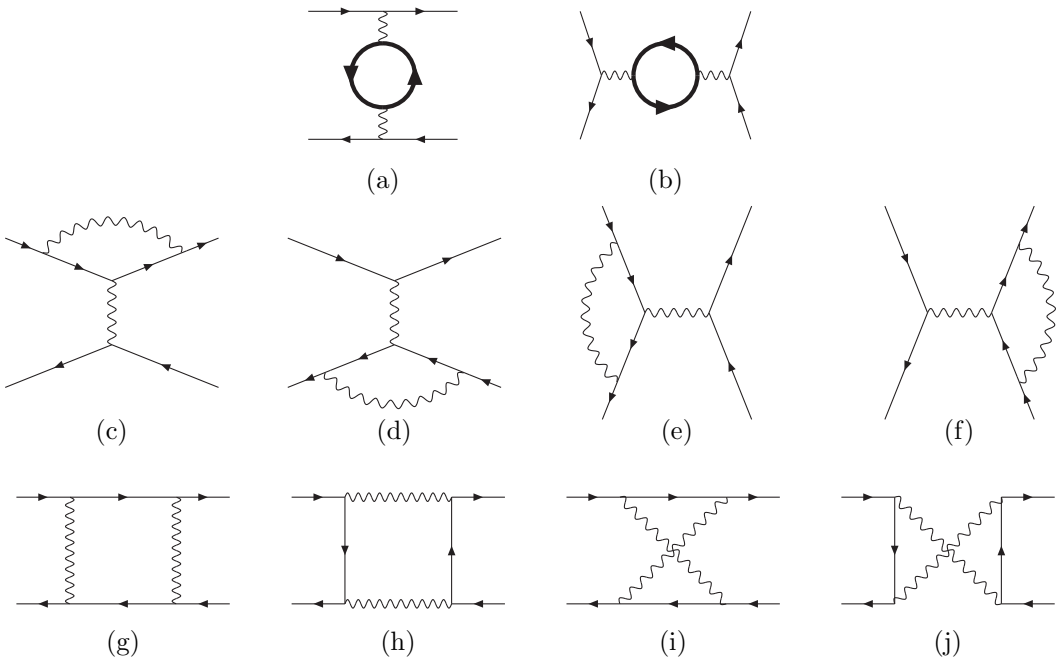

Figure 1: *One-loop diagrams.*

Eq. (5). Thus we consider the second-order contribution to the cross section given by the sum of two terms:

$$\frac{d\sigma_2}{d\Omega} = \frac{d\sigma_2^V}{d\Omega} + \frac{d\sigma_2^S}{d\Omega}\,, \tag{8}$$

which correspond to the two-loop virtual correction,[8] and the one-loop correction to the single soft photon emission which factorizes into the product of the first-order contributions [49].

The calculation of the virtual corrections is a highly nontrivial problem since in principle it involves the two-loop box diagrams depending on four mass scales: s, t, m_f, and m_e. These diagrams are beyond the reach of the available calculational techniques. However, in practice the electron mass is much smaller than any of the other mass scales involved in the problem and the calculation can be significantly simplified by exploiting this scale hierarchy. The small electron mass limit is not trivial because a finite electron mass regulates the *collinear* divergencies, giving a logarithmic dependence of the second order correction on m_e. One way to perform a systematic expansion in the small electron mass is to use the expansion by regions approach [50]. However, if we are interested only in the leading order term in m_e^2/s, the problem can be solved in an elegant way without the expansion of the individual diagrams [46]. The main idea of the method is to use the general theory of collinear divergencies to identify a set of simple diagrams responsible for the singular behavior of the corrections on the electron mass. Then, we compute the remaining corrections with a strictly massless electron, effectively removing one mass scale from the most complicated part of the calculation.

Let us describe the approach of [46] in more detail. The second order contribution to the cross section can be split in the sum of two terms according to the asymptotic dependence on

[8]We do not consider the trivial correction given by two heavy-fermion loop insertions which are are usually treated by Dyson resummation.

m_e:

$$\frac{d\sigma_2}{d\Omega} = \left[\delta_1^{(2)} \ln\left(\frac{s}{m_e^2}\right) + \delta_0^{(2)} + \mathcal{O}(m_e^2/s)\right] \frac{d\sigma_0}{d\Omega}\,. \tag{9}$$

The logarithmic term in Eq. (9) is a remnant of the collinear divergence regulated by the electron mass. The quantities $\delta_1^{(2)}$ and $\delta_0^{(2)}$ in Eq. (9) depend on s, t, and m_f only. The collinear divergencies, and hence the singular dependence of the corrections on m_e, have a peculiar structure which was extensively studied in the context of QCD. In particular, in a physical (Coulomb or axial) gauge the collinear divergencies factorize and can be absorbed in the external field renormalization [51]. Due to the factorization, the singular dependence on m_e is the same for the Bhabha amplitude and the square of the vector form factor [24]. This attributes the total logarithmic corrections to the two-loop Bhabha scattering amplitude to the one-particle reducible diagrams (s)–(v) and the one-particle irreducible diagrams (g)–(j) of Fig. 4. Moreover, due to the on-shell renormalization condition, the vacuum polarization does not change the photon propagator near the mass shell where the collinear divergencies are located. As a result, the irreducible diagrams are infrared finite even for $m_e = 0$ and the singular terms are entirely contained in the reducible diagrams. In calculating the cross section one has to take into account also the contributions coming from the interference of the one-loop corrections to the amplitude and the soft emission. Both contributions have a factorized form and can be easily evaluated for $m_e \neq 0$. Thus, it is straightforward to obtain the coefficient of the logarithmic term in Eq. (9), which reads

$$\delta_1^{(2)} = \left[2 \ln\left(\frac{4\omega^2}{s}\right) + 3\right] \frac{d\sigma_1}{d\sigma_0}\,. \tag{10}$$

At the same time the sum of the remaining two-loop one-particle irreducible diagrams has a regular behavior in the small electron mass limit and can be computed with $m_e = 0$. The two-loop vacuum polarization given by the diagrams (a)–(f) in Fig. 4 does not develop collinear singularities, because the corresponding photon is far off-shell. Hence, the sum of the two-loop box diagrams (k)–(r) in Fig. 4 is free of collinear divergencies as well. Let us emphasize that this property in general holds only for the sum of the diagrams. The individual diagrams computed in a covariant gauge do exhibit the collinear divergencies for $m_e = 0$. This, however, does not pose any additional problem since we work in dimensional regularization. In this case, the collinear divergencies show up as extra poles in $(D-4)$, which are not related to the soft emission and disappear in the sum of the one-particle irreducible diagrams. The cancellation of the collinear singularities of the box diagrams in the Feynman gauge is schematically shown in Figs. 2 and 3 for the one- and two-loop cases, respectively. Let us demonstrate this cancellation explicitly in the case of the one-loop graphs. Each one-loop box diagram for $m_e = 0$ exhibits a double pole in $(D-4)$, arising from the overlapping of soft and collinear divergencies. In particular, for the diagram (g) in Fig. 1 one finds

$$\left.\frac{d\sigma_1^V}{d\Omega}\right|_{(\mathrm{g})} = \frac{\alpha^2}{s} \frac{1}{(D-4)^2} \left[\frac{m_f^2}{s} B_1^{(1l,-2)}(s,t) + \frac{m_f^2}{t} B_2^{(1l,-2)}(s,t)\right] + \mathcal{O}(1/(D-4))\,, \tag{11}$$

while for the diagram (i) one obtains

$$\left.\frac{d\sigma_1^V}{d\Omega}\right|_{(\mathrm{i})} = \frac{\alpha^2}{s} \frac{1}{(D-4)^2} \left[\frac{m_f^2}{s} B_3^{(1l,-2)}(u,t) - \frac{m_f^2}{t} B_2^{(1l,-2)}(u,t)\right] + \mathcal{O}(1/(D-4))\,. \tag{12}$$

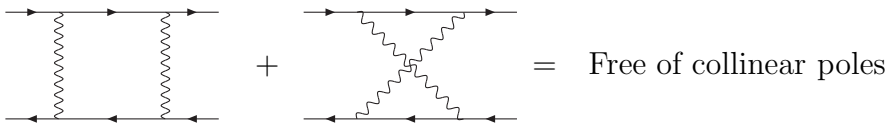

Figure 2: *Cancellation of the collinear poles among one-loop box diagrams calculated by setting* $m_e = 0$ *from the start.*

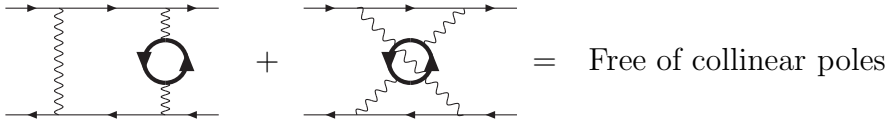

Figure 3: *Cancellation of the collinear poles among two-loop box diagrams calculated by setting* $m_e = 0$ *from the start.*

The explicit expressions of the auxiliary functions $B_i^{(1l,-2)}$ $(i = 1, 2, 3)$ for $x > 0$ are collected in Appendix B. It is easy to check that

$$\begin{aligned} B_1^{(1l,-2)}(s,t) + B_3^{(1l,-2)}(u,t) &= 0\,, \\ B_2^{(1l,-2)}(s,t) - B_2^{(1l,-2)}(u,t) &= 0\,, \end{aligned} \tag{13}$$

so that the double pole disappears in the sum of the diagrams. The residual single pole in $(D-4)$ is of soft nature and it is canceled after adding the soft-photon emission. The cancellation of the collinear poles of the two-loop box diagrams is completely analogous to the one-loop case.

Since the sum of the box diagrams has a smooth limit $m_e \to 0$, the result does not depend on whether this limit or the limit $\epsilon \to 0$ is taken first. In other words, the absence of collinear divergencies makes in such a way that the expression of the sum of the box diagrams cannot depend on which collinear regulator (electron mass or dimensional regularization) is employed in the calculation. All the "true" two-loop diagrams contribute only to the non-logarithmic term in Eq. (9) and, thus, can be evaluated for $m_e = 0$. The two-loop problem with massless electron falls in the same complexity class as the one considered in [34,35,36] and can be solved by similar approach. In the reduction of the two-loop box diagrams, however, two completely new MIs appear. The calculation of these MIs is described in the next section.

4 The Master Integrals

The two-loop heavy-fermion correction to the Bhabha scattering amplitude is given by the Feynman diagrams shown in Fig. 4. We express the square modulus of the amplitude in terms of scalar integrals. The ultraviolet, soft, and collinear divergencies of the integrals are treated by dimensional regularization. By means of the Laporta algorithm [37] the scalar integrals are reduced to six MIs diagrammatically shown in Fig. 5. Four of them, Fig. 5 (c)–(f), were already known [30,52]. The integrals Fig. 5 (a) and (b) represent the main computational result of the present paper. Below we describe their calculation.

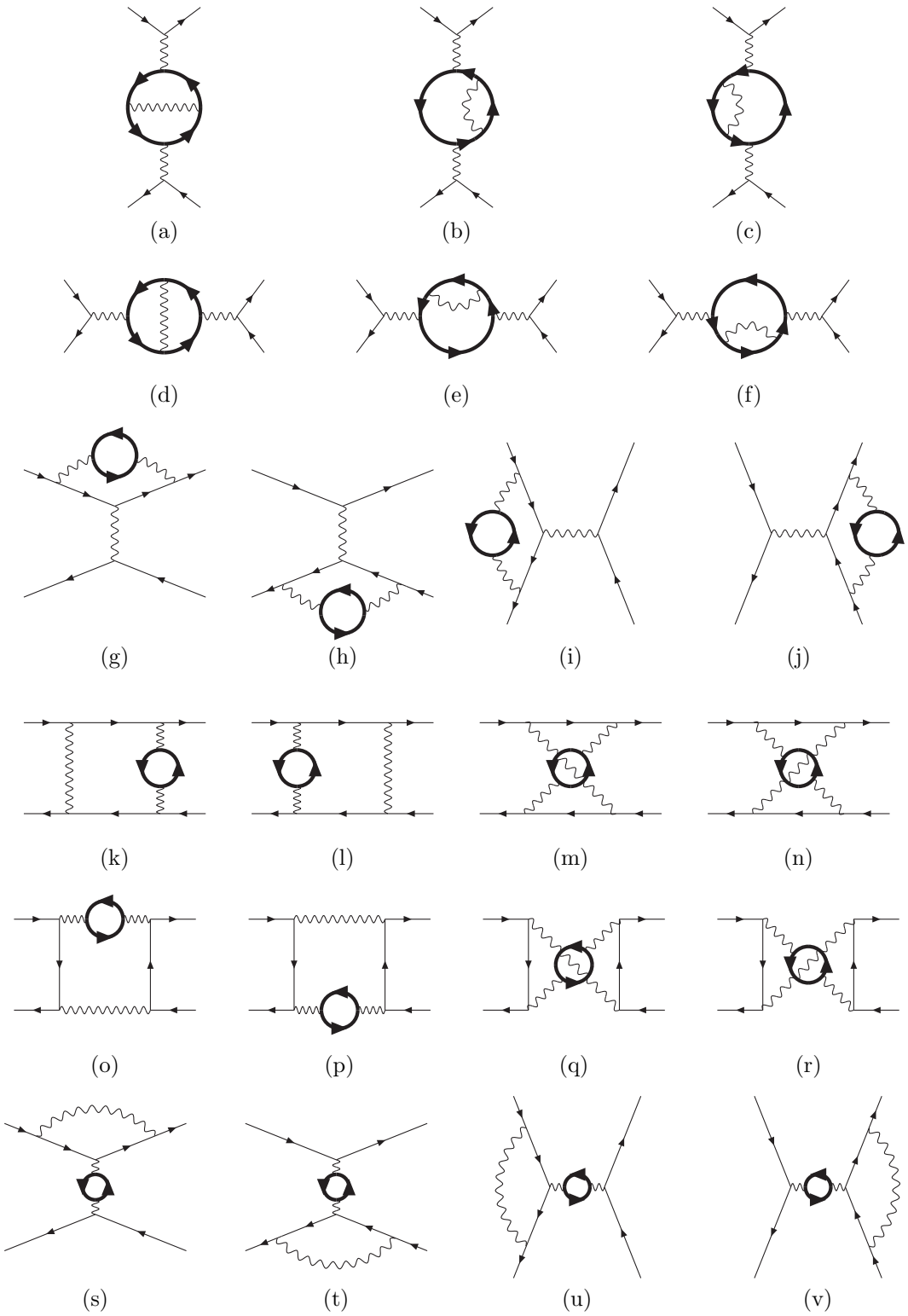

Figure 4: *Two-loop diagrams containing a heavy-flavor loop.*

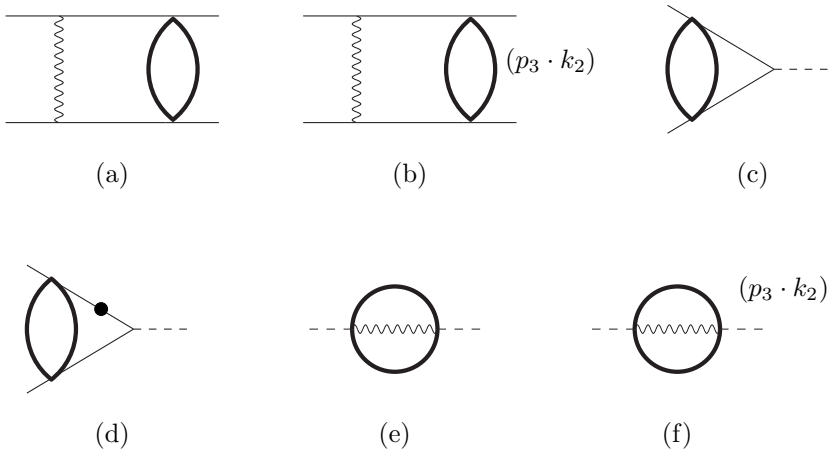

Figure 5: *The set of 6 two-loop Master Integrals involved in the calculation.*

For the pair of MIs of the box topology we choose the integrals Fig. 5 (a) and (b) with the following momentum routing:

$$M_1(D, m_f^2, P^2, Q^2) \;=\; \int \mathfrak{D}^D k_1 \mathfrak{D}^D k_2 \, \frac{1}{\mathcal{D}_1 \mathcal{D}_3 \mathcal{D}_4 \mathcal{D}_5 \mathcal{D}_6} \,, \tag{14}$$

$$M_2(D, m_f^2, P^2, Q^2) \;=\; (p_3 \cdot k_2) \;= \int \mathfrak{D}^D k_1 \mathfrak{D}^D k_2 \, \frac{p_3 \cdot k_2}{\mathcal{D}_1 \mathcal{D}_3 \mathcal{D}_4 \mathcal{D}_5 \mathcal{D}_6} \,, \tag{15}$$

where $\mathcal{D}_1 = k_1^2$, $\mathcal{D}_2 = (p_1 - k_1)^2$, $\mathcal{D}_3 = (p_2 + k_1)^2$, $\mathcal{D}_4 = k_2^2 + m_f^2$, $\mathcal{D}_5 = (p_1 - p_3 - k_1 + k_2)^2 + m_f^2$, and where the integration measure is defined as

$$\int \mathfrak{D}^D k = \frac{1}{C(D)} \left(\frac{\mu^2}{m_f^2} \right)^{\frac{(D-4)}{2}} \int \frac{d^D k}{(2\pi)^{(D-2)}} \,. \tag{16}$$

$C(D)$ is a function of the space-time dimension D:

$$C(D) = (4\pi)^{\frac{(4-D)}{2}} \Gamma\left(3 - \frac{D}{2}\right) \,, \tag{17}$$

with $C(4) = 1$. In Eq. (16) μ stands for the 't Hooft scale of dimensional regularization and we set $\mu = m_f$ in the rest of the paper. The integration measure in Eq. (16) is chosen in such a way that the one-loop massive tadpole becomes

$$\int \mathfrak{D}^D k \, \frac{1}{k^2 + m_f^2} = \frac{m_f^2}{(D-2)(D-4)} \,. \tag{18}$$

The MIs M_1 and M_2 satisfy two systems of first-order linear differential equations [39] in the external kinematical invariants s and t. With our choice of MIs, the s-system is completely

decoupled, *i.e.* every MI satisfies a single first-order linear differential equation. By contrast, the t-system consists of two coupled equations and, therefore, is equivalent to a second-order linear differential equation for one of the MIs.[9] The solution of the system requires two initial conditions. Our MIs are functions of m_f^2, s and t. They are regular for $t \to 0$ and it is possible to determine the initial conditions at $t = 0$ for any value of s. Therefore, it is more convenient to solve the system of the differential equations in t then the decoupled first-order equations in s. We define the following dimensionless variables:

$$x = \frac{P^2}{m_f^2} = -\frac{s}{m_f^2}\,, \quad y = \frac{Q^2}{m_f^2} = -\frac{t}{m_f^2}\,. \tag{19}$$

In terms of these variables the t-system takes the form:

$$\frac{dM_1}{dy} = \left[\frac{D-5}{2y} - \frac{1}{2(y+4)} - \frac{D-4}{2(y+x)}\right] M_1 + \frac{3D-10}{2m_f^2}\left[\frac{1}{y} - \frac{1}{y+4}\right] M_2 + \Omega_1(D, m_f^2, x, y), \tag{20}$$

$$\frac{dM_2}{dy} = \frac{m_f^2}{2(y+4)} M_1 - \left[\frac{D-4}{2}\left(\frac{1}{y} + \frac{1}{y+x}\right) - \frac{3D-10}{2(y+4)}\right] M_2 + \Omega_2(D, m_f^2, x, y)\,. \tag{21}$$

Note that the second MI with the scalar product on the numerator is dimensionless, while the first one has the mass dimension of m_f^{-2}. The functions $\Omega_i(D, m_f^2, x, y)$ are linear combinations of the MIs (c)–(f) of Fig. 5, the product of a massless one-loop bubble and a massive tadpole, and the product of two tadpoles:

$$\begin{aligned}
\Omega_1 \;=\; & \frac{x(x-4)}{y(4+y)(x+y)} \quad \text{ 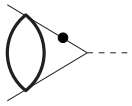 } \\
& -\frac{1}{2m_f^4(D-4)y^2(y+4)^2(y+x)}(-560 + 384D - 64D^2 + 200x - 140Dx + 24D^2x \\
& \quad +72y - 76Dy + 16D^2y + 10Dxy - 3D^2xy + 48y^2 - 40Dy^2 + 8D^2y^2) \quad \text{ 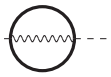 } \\
& +\frac{12(D-2)(-28 + 8D + 10x - 3Dx - 6y + 2Dy)}{m_f^6(D-4)y^2(y+4)^2(y+x)} \quad \text{ 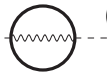 } \; (p_3 \cdot k_2) \\
& +\frac{2(D-2)(D-3)}{m_f^4(D-4)xy(y+4)} \quad \text{ 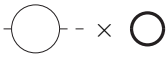 } \\
& -\frac{(D-2)}{8m_f^6(D-5)(D-4)(D-3)y^2(y+4)^2(y+x)}(5600 - 4960D + 1408D^2 - 128D^3 \\
& \quad -2000x + 1800Dx - 520D^2x + 48D^3x + 1184y - 1096Dy + 328D^2y - 32D^3y \\
& \quad -296xy + 304Dxy - 98D^2xy + 10D^3xy - 24y^2 + 20Dy^2 - 4D^2y^2 - 24xy^2 \\
& \quad +26Dxy^2 - 9D^2xy^2 + D^3xy^2) \quad \text{  }\,,
\end{aligned} \tag{22}$$

$$\begin{aligned}
\Omega_2 \;=\; & \frac{(D-4)x}{8y(y+x)} \quad \text{ 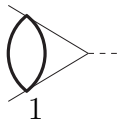 } \quad + \frac{m_f^2 x(x-4)}{4(y+4)(y+x)} \quad \text{ 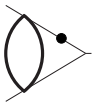 } \\
& -\frac{1}{4m_f^2(D-4)y^2(y+4)^2(y+x)}(-360x + 224Dx - 32D^2x - 480y + 312Dy - 48D^2y
\end{aligned}$$

[9] As it is shown below, the second-order equation in t turns out to be particularly simple because the system of the first-order equations in s is decoupled.

$$
\begin{aligned}
&+16xy - 34Dxy + 8D^2xy - 8y^2 - 20Dy^2 + 6D^2y^2 + 24xy^2 - 21Dxy^2 + 4D^2xy^2 \\
&+48y^3 - 44Dy^3 + 9D^2y^3) \quad \text{--}\!\!\bigcirc\!\!\text{--} \\
&-\frac{6(D-2)(18x-4Dx+24y-6Dy+4xy-Dxy+10y^2-3Dy^2)}{m_f^4(D-4)y^2(y+4)^2(y+x)} \quad \text{--}\!\!\bigcirc\!\!\text{--} \; (p_3\cdot k_2) \\
&+\frac{(D-3)(D-2)}{2m_f^2(D-4)x(y+4)} \quad \text{--}\!\!\bigcirc\!\!\text{--} \times \bigcirc \\
&-\frac{D-2}{32m_f^4(D-5)(D-4)(D-3)y^2(y+4)^2(y+x)}(7200x - 5920Dx + 1536D^2x \\
&-128D^3x + 9600y - 8160Dy + 2208D^2y - 192D^3y + 1360xy - 1032Dxy \\
&+232D^2xy - 16D^3xy + 3424y^2 - 2944Dy^2 + 808D^2y^2 - 72D^3y^2 - 176xy^2 \\
&+200Dxy^2 - 72D^2xy^2 + 8D^3xy^2 + 16y^3 - 8Dy^3 - 24xy^3 + 26Dxy^3 - 9D^2xy^3 \\
&+D^3xy^3) \quad \bigcirc\!\!\bigcirc \quad . \qquad (23)
\end{aligned}
$$

All the possible singularities of the integrals M_1 and M_2 are those appearing in their coefficients in Eqs. (20,21). Thus, the singularities are potentially located at $y = 0$, $y = -4$ and $y = -x$. The point $y = -4$ is a singular point for the integrals. It corresponds to the three (two massive and one massless) particle cut in the t channel. By contrast, $y = 0$ is a regular point. We can use this information in order to determine the initial conditions. In fact, multiplying Eqs. (20, 21) by y and taking into account that $y\, dM_{1,2}/dy|_{y\to 0} \to 0$, in the limit $y \to 0$ we find

$$
\begin{aligned}
M_1(D,x,y=0) &= -\frac{1}{2m_f^2x}\frac{1}{(D-4)^3} - \frac{G(0,x)}{4m_f^2x}\frac{1}{(D-4)^2} + \frac{\zeta(2)-G(0,0,x)}{8m_f^2x}\frac{1}{(D-4)} \\
&+\frac{1}{16m_f^2x}[8 - 2\zeta(3) + (\zeta(2)-4)G(0,x) - G(0,0,0,x) + G(\mu,\mu,0,x)] \\
&+\frac{4-x}{8m_f^2x\sqrt{x(4-x)}}G(\mu,0,x) + \mathcal{O}(D-4)\,, \qquad (24) \\
M_2(D,x,y=0) &= \frac{1}{16}\frac{1}{(D-4)^2} - \frac{(2-G(0,x))}{32}\frac{1}{(D-4)} + \frac{1}{64x}[11x - \zeta(2)x - 5xG(0,x) \\
&+xG(0,0,x) + 2G(\mu,\mu,0,x)] + \frac{4-x}{64\sqrt{x(4-x)}}G(\mu,0,x) + \mathcal{O}(D-4)\,, \qquad (25)
\end{aligned}
$$

where the functions G are generalized harmonic polylogarithms (GHPLs) [53] described in Appendix A. The system of Eqs. (20,21) is equivalent to a second-order linear differential equation for one of the MIs. For the integral M_1, after trivial manipulations, we find

$$
\begin{aligned}
&\frac{d^2M_1}{dy^2} + \left[\frac{3}{2y} - \frac{3D-13}{2(y+4)} + \frac{D-4}{y+x}\right]\frac{dM_1}{dy} - (D-4)\left[\frac{D-5}{4y^2} - \left(\frac{3D-17}{16} + \frac{3}{4x}\right)\frac{1}{y}\right. \\
&\left. -\frac{D-6}{4(y+x)^2} + \left(\frac{3}{4x} - \frac{3D-13}{4(x-4)}\right)\frac{1}{y+x} + \left(\frac{3D-17}{16} + \frac{3D-13}{4(x-4)}\right)\frac{1}{y+4}\right]M_1 \\
&+\Omega(D,m_f^2,x,y) = 0\,. \qquad (26)
\end{aligned}
$$

The function $\Omega(D, m_f^2, x, y)$ contains the MIs (c)–(f) of Fig. 5, some products of one-loop integrals and the product of two tadpoles.

Let us discuss briefly the structure of the Eq. (26). Note that we are not interested in a solution of the differential equation valid for arbitrary value of the space-time parameter D. Instead, we look for a solution in the form of a Laurent series in $(D-4)$. Since the coefficient of M_1 is proportional to $(D-4)$, Eq. (26) at each order in $(D-4)$ is reduced to a first-order linear differential equation for the derivative $M_1' = dM_1/dy$:

$$M_1'(D, m_f^2, x, y) = \sum_{i=-3}^{N} M_{1,i}' \, (D-4)^i + \mathcal{O}(D-4)^{N+1} \,, \tag{27}$$

$$\frac{dM_{1,i}'}{dy} = -\left[\frac{3}{2y} + \frac{1}{2(y+4)}\right] M_{1,i}' + \Psi_i(m_f^2, x, y) \,. \tag{28}$$

The functions $\Psi_i(m_f^2, x, y)$ in Eq. (28) are defined as follows ($M_{1,j} = 0$ for $j < -3$):

$$\begin{aligned}
\Psi_i(m_f^2, x, y) &= -\Omega_i(D, m_f^2, x, y) + \left[\frac{3}{2(y+4)} - \frac{1}{y+x}\right] M_{1,i-1}' - \left[\frac{1}{4y^2} + \left(\frac{3}{4x} - \frac{5}{16}\right)\frac{1}{y}\right. \\
&\left. - \frac{1}{2(y+x)^2} - \left(\frac{3}{4x} + \frac{1}{4(x-4)}\right)\frac{1}{y+x} + \left(\frac{5}{16} + \frac{1}{4(x-4)}\right)\frac{1}{y+4}\right] M_{1,i-1} \\
&+ \left[\frac{1}{4y^2} - \frac{3}{16y} - \frac{1}{4(y+x)^2} - \frac{3}{4(x-4)}\,\frac{1}{y+x}\right. \\
&\left. + \left(\frac{3}{16} + \frac{3}{4(x-4)}\right)\frac{1}{y+4}\right] M_{1,i-2} \,.
\end{aligned} \tag{29}$$

Note that $\Psi_i(m_f^2, x, y)$ contains $M_{1,i-1}'$, $M_{1,i-1}$ and $M_{1,i-2}$. Moreover, $\Psi_i(m_f^2, x, y)$ contains the i-th order term of the Laurent expansion of $\Omega(D, m_f^2, x, y)$:

$$\begin{aligned}
\Omega(D, m_f^2, x, y) &= \sum_{i=-2}^{0} \Omega_i(D, m_f^2, x, y) \, (D-4)^i + \mathcal{O}(D-4) \,, \\
&= \frac{2x^2 + 10xy - x^2y + 4y^2}{4m_f^2 xy^2(4+y)(x+y)^2} \, \frac{1}{(D-4)^2} \\
&- \frac{1}{8m_f^2 y^2 (x+y)^2}\left[\frac{8x + 20y - 2xy + y^2}{(4+y)} - \frac{2x^2 + 10xy - x^2y + 4y^2}{x(4+y)} G(0,x)\right. \\
&\left. - \frac{2x + 6y - xy}{\sqrt{y(y+4)}} G(-\mu, y)\right] \frac{1}{(D-4)} \\
&+ \frac{1}{16m_f^2 y^2 (x+y)^2 x(4+y)} \Big\{ 16x^2 + 40xy - 4x^2y + 2xy^2 - 2x^2\zeta(2) \\
&- 10xy\zeta(2) + x^2y\zeta(2) - 4y^2\zeta(2) - x(4x + 16y - 3xy) G(0,x) + (2x^2 \\
&+ 10xy - x^2y + 4y^2) G(0,0,x) + 2x(2x - 2y + xy) G(-\mu, -\mu, y) \\
&+ \frac{xy(x-4)^2}{\sqrt{x(4-x)}} G(\mu, 0, x) - \frac{x(y+4)}{\sqrt{y(y+4)}} \Big[(12x + 24y - xy + 2y^2) G(-\mu, y) \\
&- (2x + 6y - xy) G(0, -\mu, y) - 3(2x + 6y - xy) G(-4, -\mu, y) \Big] \Big\} \\
&+ \mathcal{O}(D-4) \,.
\end{aligned} \tag{30}$$

The formal solution of Eq. (28) reads

$$M'_{1,i} = \frac{1}{y\sqrt{y(y+4)}} \left[\int^y r\sqrt{r(r+4)}\Psi_i \, dr + J_i \right] , \tag{31}$$

where J_i are integration constants, which are fixed by the regularity condition for the derivative $M'_{1,i}$ at $y = 0$. Actually, in every order in $(D-4)$ we find $J_i = 0$. This means that we have to discard the homogeneous solution and keep only the particular solution of the inhomogeneous Eq. (28). Then, we integrate Eq. (31):

$$M_{1,i} = \int^y M'_{1,i}(m_f^2, x, r) \, dr + J_{1,i} \, . \tag{32}$$

$J_{1,i}$ are again integration constants which are determined by the initial conditions Eq. (24). Once we have the master integral M_1, the calculation of M_2 is straightforward. From Eq. (20), we express M_2 in terms of M_1 and dM_1/dy. The final analytical expression for M_1 and M_2 reads

$$M_1(D, m_f^2, x; y) = \sum_{i=-3}^{0} M_{1,i}(m_f^2, x; y) \, (D-4)^i + \mathcal{O}(D-4) \, , \tag{33}$$

where

$$M_{1,-3} = -\frac{1}{2m_f^2 x} \, , \tag{34}$$

$$M_{1,-2} = \frac{1}{4m_f^2 x} \left[2 - G(0;x) - \frac{y+4}{\sqrt{y(y+4)}} G(-\mu; y) \right] , \tag{35}$$

$$\begin{aligned} M_{1,-1} = {} & \frac{1}{8m_f^2 x} \Bigg\{ -4 + \zeta(2) + 2G(0;x) - G(0,0;x) + 2G(-\mu,-\mu;y) \\ & + \frac{y+4}{\sqrt{y(y+4)}} \Big[2G(-\mu;y) - 3G(-4,-\mu;y) - G(0;x)G(-\mu;y) \Big] \Bigg\} , \end{aligned} \tag{36}$$

$$\begin{aligned} M_{1,0} = {} & -\frac{(x-4)(y+4)}{16m_f^2\sqrt{x(4-x)}\sqrt{y(y+4)}} G(\mu, 0; x) G(-x-\mu; y) \\ & + \frac{4+y}{16m_f^2 x\sqrt{y(y+4)}} [-G(-x, 0, -\mu; y) + 6G(-\mu, -\mu, -\mu; y) - (4 - \zeta(2)) G(-\mu; y) \\ & + G(0;x)(-3G(-4,-\mu;y) + G(-x,-\mu;y) + 2G(-\mu;y) - G(0,-\mu;y)) \\ & + 6G(-4,-\mu;y) - 9G(-4,-4,-\mu;y) + G(0,0,-\mu;y) - G(0,0;x)G(-\mu;y)] \\ & + \frac{1}{16m_f^2 x} [8 - 2\zeta(2) - 2\zeta(3) - 4G(-\mu,-\mu;y) + 6G(-\mu,-4,-\mu;y) + G(\mu,\mu,0;x) \\ & - 4G(0,-\mu,-\mu;y) - (4-\zeta(2))G(0;x) + 2G(0;x)G(-\mu,-\mu;y) + 2G(0,0;x) \\ & - G(0,0,0;x)] \, , \end{aligned} \tag{37}$$

and

$$M_2(D, m_f^2, x; y) = \sum_{i=-3}^{0} M_{2,i}(m_f^2, x; y) \, (D-4)^i + \mathcal{O}(D-4) \, , \tag{38}$$

where

$$M_{2,-3} = -\frac{y}{8x}\,, \tag{39}$$

$$M_{2,-2} = \frac{1}{16x}\left[x + y(4 - G(0;x)) - \frac{y(y+4)}{\sqrt{y(y+4)}}G(-\mu;y)\right]\,, \tag{40}$$

$$\begin{aligned} M_{2,-1} &= \frac{1}{32x}\left[\zeta(2)y - 5x - 14y + 2\Big(2+y+\frac{x}{y}\Big)G(-\mu,-\mu;y) + (x+4y)G(0;x) - yG(0,0;x)\right] \\ &+\frac{4+y}{32x\sqrt{y(y+4)}}[(x+4y)G(-\mu;y) - 3yG(-4,-\mu;y) - yG(0;x)G(-\mu;y)]\,, \end{aligned} \tag{41}$$

$$\begin{aligned} M_{2,0} &= -\frac{y(y+4)(x-4)}{64\sqrt{x(4-x)}\sqrt{y(y+4)}}G(\mu,0;x)G(-x-\mu;y) - \frac{x-4}{64\sqrt{x(4-x)}}G(mu,0;x) \\ &+\frac{y(y+4)}{64x\sqrt{y(y+4)}}\Big[-G(-x,0,-\mu;y) + \Big(\zeta(2) - 14 - \frac{5x}{y}\Big)G(-\mu;y) \\ &+\Big(12 + \frac{3x}{y}\Big)G(-4,-\mu;y) + 6G(-\mu,-\mu,-\mu;y) - 9G(-4,-4,-\mu;y) \\ &+\frac{x}{y}G(0,-\mu;y) + G(0,0,-\mu;y) + G(0;x)(G(-x,-\mu;y) - 3G(-4,-\mu;y) \\ &+4G(-\mu;y) - G(0,-\mu;y)) - G(0,0;x)G(-\mu;y)\Big] + \frac{1}{64x}\Big[19x + 46y - \zeta(2)x \\ &-4\zeta(2)y - 2\zeta(3)y - 2\Big(6 + 3\frac{x}{y} + x + 4y\Big)G(-\mu,-\mu;y) \\ &+6\Big(2 + \frac{x}{y} + y\Big)G(-\mu,-4,-\mu;y) + \frac{2x}{y}G(-\mu,0,-\mu;y) + (2+y)G(\mu,\mu,0;x) \\ &-2\Big(4 + \frac{x}{y} + 2y\Big)G(0,-\mu,-\mu;y) + 2(2+y)G(0;x)G(-\mu,-\mu;y) \\ &+(\zeta(2)y - 5x - 14y)G(0;x) + (x+4y)G(0,0;x) - yG(0,0,0;x)\Big]\,, \end{aligned} \tag{42}$$

The result is expressed in terms of GHPLs of two variables, x and y. More details on these functions can be found in Appendix A. We checked that Eqs. (33,38) do satisfy the system of linear differential equations in s, and the initial condition of Eq. (25) for M_2 is recovered in the limit $x \to 0$.

5 The Two-Loop Heavy-Flavor Correction

In this Section we present the analytical result for the contribution of the different classes of the two-loop diagrams shown in Fig. 4 and the corresponding soft-photon emission contribution to the differential cross section. We keep the notations as close as possible to [35,36]. The ultraviolet divergencies are renormalized in the on-shell scheme.

It is convenient to split the two-loop virtual correction in Eq. (8) into the sum of five terms

$$\frac{d\sigma_2^V}{d\Omega} = \frac{d\sigma_2^V}{d\Omega}\Big|_{(2l,S)} + \frac{d\sigma_2^V}{d\Omega}\Big|_{(2l,V)} + \frac{d\sigma_2^V}{d\Omega}\Big|_{(2l,B)} + \frac{d\sigma_2^V}{d\Omega}\Big|_{(2l,R)} + \frac{d\sigma_2^V}{d\Omega}\Big|_{(S,V)} + \frac{d\sigma_2^V}{d\Omega}\Big|_{(S,B)}\,, \tag{43}$$

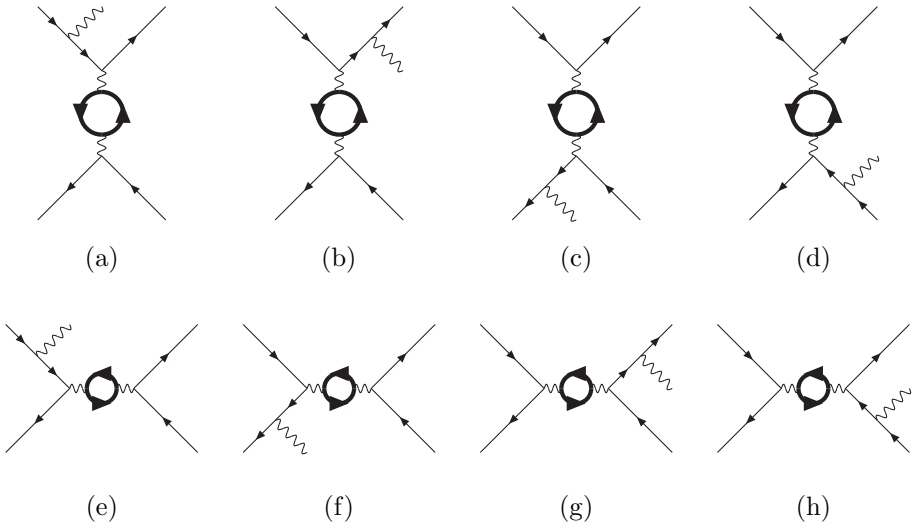

Figure 6: *Diagrams contributing to the real corrections to the NNLO heavy flavor cross section.*

which correspond to the contribution of the two-loop self-energy diagrams, two-loop vertex diagrams, two-loop box diagrams, two-loop reducible diagrams, and to the interference of one-loop vertex and one-loop box diagrams with the one-loop self-energy diagrams, respectively. We drop the list of arguments of the various contributions to the cross section. All the terms in Eq. (43) depend on s, t, and m_f. As it is explained in Section 3, only the fourth and fifth terms on the r. h. s. of Eq. (43) depend logarithmically on the electron mass m_e.

5.1 Two-Loop Vacuum Polarization Corrections

The contribution of the diagrams Fig. 4 (a)–(f) can be obtained by replacing $\Pi_0^{(1l)}$ with the two-loop vacuum polarization function $\Pi_0^{(2l)}$ in Eq. (7):

$$\begin{aligned}\left.\frac{d\sigma_2^V}{d\Omega}\right|_{(2l,S)} &= \frac{\alpha^2}{s}Q_f^4 N_c\left\{\frac{1}{s^2}\left[st+\frac{s^2}{2}+t^2\right]2\mathrm{Re}\Pi_0^{(2l)}(s)+\frac{1}{t^2}\left[st+\frac{t^2}{2}+s^2\right]2\Pi_0^{(2l)}(t)\right.\\ &\left.+\frac{1}{st}(s+t)^2\left(\mathrm{Re}\Pi_0^{(2l)}(s)+\Pi_0^{(2l)}(t)\right)\right\}. \end{aligned} \tag{44}$$

The explicit expression of the renormalized function $\Pi_0^{(2l)}$ in terms of GHPLs is given in Eq. (162) of Appendix B. Note that the two-loop vacuum polarization corrections are proportional to the fourth power of the heavy fermion charge, while all the other corrections are proportional to Q_f^2.

5.2 Two-Loop Vertex Corrections

The two-loop vertex diagram are shown in Fig. 4 (g)–(j). These diagrams are infrared finite and can be evaluated for $m_e = 0$. The analytical result for the two-loop vertex correction reads

$$\left.\frac{d\sigma_2^V}{d\Omega}\right|_{(2l,V)} = 2\frac{\alpha^2}{s}Q_f^2 N_c\left[\frac{1}{s^2}V_2^{(2l)}(t,s)+\frac{1}{t^2}V_2^{(2l)}(s,t)+\frac{1}{st}\left(V_1^{(2l)}(s,t)+V_1^{(2l)}(t,s)\right)\right]. \tag{45}$$

The functions $V_1^{(2l)}$ and $V_2^{(2l)}$ in this equation are related to the two-loop Dirac form factor[10] $F_1^{(2l)}(-p^2)$ as follows:

$$V_1^{(2l)}(s,t) = c_{1,1}(s,t)\mathrm{Re}F_1^{(2l)}(t)\,, \tag{46}$$

$$V_2^{(2l)}(s,t) = c_{2,1}(s,t)\mathrm{Re}F_1^{(2l)}(t)\,, \tag{47}$$

where the coefficients $c_{i,1}(s,t)$ read

$$c_{1,1}(s,t) = (s+t)^2\,, \quad c_{2,1}(s,t) = 2\left(st+s^2+\frac{t^2}{2}\right)\,. \tag{48}$$

The explicit expressions of the renormalized form factor is given in Eq. (179) of Appendix B.

5.3 Two-Loop Box Corrections

There are eight two-loop box diagrams shown in Fig. 4 (k)–(r). If we transform the external momenta $p_4 \leftrightarrow -p_1$ and $p_2 \leftrightarrow -p_3$ in the diagram (l), it becomes identical to the diagram (k). Since this transformation does not change the Mandelstam variables s and t, the contributions of diagrams (k) and (l) to the differential cross section are equal. The same is true for the pairs of diagrams: (m)-(n), (o)-(p), and (q)-(r). Thus the contribution of the two-loop box diagrams can be written as follows:

$$\begin{aligned}\frac{d\sigma_2^V}{d\Omega}\Big|_{(2l,B)} = -2\frac{\alpha^2}{4s}Q_f^2N_c\Big[&\frac{m_f^2}{s}\Big(\mathrm{Re}B_1^{(2l)}(s,t)+\mathrm{Re}B_2^{(2l)}(t,s)+B_3^{(2l)}(u,t)-\mathrm{Re}B_2^{(2l)}(u,s)\Big)\\ &+\frac{m_f^2}{t}\Big(\mathrm{Re}B_2^{(2l)}(s,t)+\mathrm{Re}B_1^{(2l)}(t,s)-B_2^{(2l)}(u,t)+\mathrm{Re}B_3^{(2l)}(u,s)\Big)\Big]\,,\end{aligned} \tag{49}$$

where the overall minus sign is due to the closed fermion loop and the overall factor 2 reflects the identity of the diagrams discussed above. The Laurent expansion of the renormalized functions $B_i^{(2l)}$ reads

$$B_i^{(2l)}(s,t) = \frac{1}{(D-4)^2}B_i^{(2l,-2)}(s,t)+\frac{1}{(D-4)}B_i^{(2l,-1)}(s,t)+B_i^{(2l,0)}(s,t)+\mathcal{O}\Big((D-4)\Big)\,. \tag{50}$$

The expressions of the coefficients $B_i^{(2l,j)}$ for $j=-2,-1,0$, are given in Eqs. (181–189) of Appendix B. As it was pointed out in Section 3, the double poles of the auxiliary functions $B_i^{(2l,j)}$ cancel in the sum of the planar and crossed box contributions.

5.4 Two-Loop Reducible Corrections

The two-loop reducible diagrams are shown in Fig. 4 (s)–(v). They reduce to the product of the one-loop vacuum polarization function and one-loop Dirac form factor and can be easily obtained from Eq. (43) of [35]. The result is of the following form:

$$\frac{d\sigma_2^V}{d\Omega}\Big|_{(2l,R)} = 2\frac{\alpha^2}{s}Q_f^2N_c\left[\frac{1}{s^2}V_2^R(t,s)+\frac{1}{t^2}V_2^R(s,t)+\frac{1}{st}\left(V_1^R(s,t)+V_1^R(t,s)\right)\right]\,, \tag{51}$$

[10]The Pauli form factor vanishes in the limit $m_e \to 0$.

where the functions $V_i^R(s,t)$ have the Laurent expansion

$$V_i^{(R)}(s,t) = \frac{1}{(D-4)} V_i^{(R,-1)}(s,t) + V_i^{(R,0)}(s,t) + \mathcal{O}\Big((D-4)\Big) \,, \tag{52}$$

with

$$\begin{aligned} V_i^{(R,-1)}(s,t) &= c_{i,1}(s,t)\ \mathrm{Re}\Big(\ F_1^{(1l,-1)}(t)\ \Pi_0^{(1l,0)}(t)\ \Big)\,, & (53)\\ V_i^{(R,0)}(s,t) &= c_{i,1}(s,t)\ \mathrm{Re}\Big(\ F_1^{(1l,0)}(t)\ \Pi_0^{(1l,0)}(t) + F_1^{(1l,-1)}(t)\ \Pi_0^{(1l,1)}(t)\ \Big) \\ &\quad + c_{i,2}(s,t)\ \mathrm{Re}\Big(\ F_1^{(1l,-1)}(t)\ \Pi_0^{(1l,0)}(t)\ \Big)\,. & (54) \end{aligned}$$

The coefficients $c_{1,1}(s,t)$ and $c_{2,1}(s,t)$ are given in Eq. (48). Moreover, we have:

$$c_{1,2}(s,t) = \frac{1}{2}(st + s^2 + t^2)\ , \qquad c_{2,2}(s,t) = \frac{1}{2}t^2\,. \tag{55}$$

In Eqs. (53,54) the quantities $\Pi^{(1l,i)}$ $(i = 0,\ 1)$ and $F_1^{(1l,i)}$ $(i = -1,\ 0)$ are the coefficients of the Laurent expansion of the one-loop vacuum polarization function and one-loop Dirac form factor given in Eqs. (161, 162) and Eqs. (164, 165) of Appendix B, respectively. Note that the form factor should be calculated by keeping a nonzero electron mass as collinear regulator.

5.5 Interference of Two One-Loop Graphs

Finally, we discuss the interference between the one-loop vacuum polarization diagrams of Fig. 1 (a) and (b), and the one-loop vertex and box diagrams of Fig. 1 (c)–(j). The calculation is straightforward because the one-loop vacuum polarization factorizes with respect to the tree-level amplitude and the interference term can be obtained from the one-loop vertex and box corrections to the cross section. For the vertex diagrams we obtain

$$\begin{aligned} \frac{d\sigma_2^V}{d\Omega}\Big|_{(S,V)} &= 2\frac{\alpha^2}{s} Q_f^2 N_c \mathrm{Re}\Bigg[\frac{1}{s^2} V_2^{(1l)}(t,s)\Big(\Pi_0^{(1l)}(s)\Big)^* + \frac{1}{t^2} V_2^{(1l)}(s,t)\Big(\Pi_0^{(1l)}(t)\Big)^* \\ &\quad + \frac{1}{st} V_1^{(1l)}(s,t)\Big(\Pi_0^{(1l)}(s)\Big)^* + \frac{1}{st} V_1^{(1l)}(t,s)\Big(\Pi_0^{(1l)}(t)\Big)^*\Bigg]\,, \end{aligned} \tag{56}$$

where the functions $V_i^{(1l)}(s,t)$ are defined as

$$\begin{aligned} V_1^{(1l)}(s,t) &= \left[2\left(st + \frac{1}{2}s^2 + \frac{1}{2}t^2\right) + \frac{1}{2}(D-4)(st + s^2 + t^2)\right] \mathrm{Re}F_1^{(1l)}(t)\,, & (57)\\ V_2^{(1l)}(s,t) &= \left[2\left(st + s^2 + \frac{1}{2}t^2\right) + \frac{1}{2}(D-4)t^2\right] \mathrm{Re}F_1^{(1l)}(t)\,. & (58) \end{aligned}$$

Their Laurent expansions read

$$V_i^{(1l)}(s,t) = \frac{1}{(D-4)} V_i^{(1l,-1)}(s,t) + V_i^{(1l,0)}(s,t) + \mathcal{O}\Big((D-4)\Big)\,, \tag{59}$$

where

$$V_i^{(1l,-1)}(s,t) = c_{i,1}(s,t)\mathrm{Re}F_1^{(1l,-1)}(t)\,, \tag{60}$$

$$V_i^{(1l,0)}(s,t) = c_{i,1}(s,t)\mathrm{Re}F_1^{(1l,0)}(t) + c_{i,2}(s,t)\mathrm{Re}F_1^{(1l,-1)}(t)\,, \tag{61}$$

and with the coefficients $c_{i,j}(s,t)$ given in Eqs. (48,55). Thus, if for instance we consider the the first term of Eq. (56), we obtain

$$\begin{aligned} V_2^{(1l)}(t,s)\Big(\Pi_0^{(1l)}(s)\Big)^* &= \frac{1}{(D-4)}V_2^{(1l,-1)}(t,s)\Big(\Pi_0^{(1l,0)}(s)\Big)^* + V_2^{(1l,0)}(t,s)\Big(\Pi_0^{(1l,0)}(s)\Big)^* \\ &\quad + V_2^{(1l,-1)}(t,s)\Big(\Pi_0^{(1l,1)}(s)\Big)^* + \mathcal{O}\Big((D-4)\Big)\,. \end{aligned} \tag{62}$$

Similar expressions hold for the other terms.

For the box diagrams we obtain

$$\begin{aligned} \frac{d\sigma_2^V}{d\Omega}\Big|_{(S,B)} = \frac{\alpha^2}{4s}Q_f^2N_c\mathrm{Re}\Bigg[&\frac{m_f^2}{s}\Big(B_1^{(1l)}(s,t)+B_2^{(1l)}(t,s)+B_3^{(1l)}(u,t)-B_2^{(1l)}(u,s)\Big)\Big(\Pi_0^{(1l)}(s)\Big)^* \\ &+\frac{m_f^2}{t}\Big(B_2^{(1l)}(s,t)+B_1^{(1l)}(t,s)-B_2^{(1l)}(u,t)+B_3^{(1l)}(u,s)\Big)\Big(\Pi_0^{(1l)}(t)\Big)^*\Bigg]\,, \end{aligned} \tag{63}$$

where the functions $B_i^{(1l)}(s,t)$ $(i=1,2,3)$ have the Laurent expansion:

$$B_i^{(1l)}(s,t) = \frac{1}{(D-4)^2}B_i^{(1l,-2)}(s,t) + \frac{1}{(D-4)}B_i^{(1l,-1)}(s,t) + B_i^{(1l,0)}(s,t) + \mathcal{O}\left((D-4)\right)\,, \tag{64}$$

The explicit expressions of the coefficients of the Laurent expansion can be found in Appendix B. Thus, for instance for the first term in Eq. (63) we obtain

$$\begin{aligned} B_1^{(1l)}(s,t)\Big(\Pi_0^{(1l)}(s)\Big)^* &= \frac{1}{(D-4)}B_1^{(1l,-1)}(s,t)\Big(\Pi_0^{(1l,0)}(s)\Big)^* + B_1^{(1l,0)}(s,t)\Big(\Pi_0^{(1l,0)}(s)\Big)^* \\ &\quad + B_1^{(1l,-1)}(s,t)\Big(\Pi_0^{(1l,1)}(s)\Big)^* + \mathcal{O}\Big((D-4)\Big)\,, \end{aligned} \tag{65}$$

and similar expressions for the other terms.

5.6 Soft Photon Emission

Let us now discuss the calculation of the second term in Eq. (8). We use the procedure applied in [36] to the case of the electron vacuum polarization. It is convenient to introduce the quantity

$$\frac{d\sigma_1^D}{d\Omega}\Big|_{(1l,S)} = \frac{d\sigma_1}{d\Omega} + (D-4)\frac{d\sigma_1^{(D-4)}}{d\Omega}\,, \tag{66}$$

where the first term on the right hand side (r.h.s.) is defined in Eq. (7) and the second term for $m_e = 0$ reads

$$\begin{aligned} \frac{d\sigma_1^{(D-4)}}{d\Omega}\Big|_{(1l,S)} = \frac{\alpha^2}{s}Q_f^2N_c\Bigg\{&\frac{1}{s^2}\left[st+\frac{s^2}{2}+t^2\right]2\mathrm{Re}\Pi_0^{(1l,1)}(s) + \frac{1}{t^2}\left[st+\frac{t^2}{2}+s^2\right]2\Pi_0^{(1l,1)}(t) \\ &+\frac{1}{st}(s+t)^2\left(\mathrm{Re}\Pi_0^{(1l,1)}(s)+\Pi_0^{(1l,1)}(t)\right) + \frac{\mathrm{Re}\Pi_0^{(1l,0)}(s)+\Pi_0^{(1l,0)}(t)}{2} \\ &+\frac{1}{2}\left[(s+t)^2-st\right]\left(\mathrm{Re}\Pi_0^{(1l,0)}(s)+\Pi_0^{(1l,0)}(t)\right)\Bigg\}\,. \end{aligned} \tag{67}$$

The contribution of the soft-photon emission is then given by

$$\frac{d\sigma_2^S}{d\Omega} = \left(\frac{d\sigma_1^D}{d\Omega}\right) 4\sum_{j=1}^{4} J_{1j}(p_1\cdot p_j, m_e^2, m_f^2)\,. \tag{68}$$

Here, the infrared divergent quantities J_{1j} $(j = 1, \cdots, 4)$ are defined as follows:

$$J_{1j}(p_1\cdot p_j, m_e^2, m_f^2) = \epsilon_j\ (p_1\cdot p_j)\ I_{1j}(p_1\cdot p_j, m_e^2, m_f^2)\,, \tag{69}$$

where $\epsilon_j = +1$ for $j = 1, 4$, $\epsilon_j = -1$ for $j = 2, 3$, and

$$I_{1j}(p_1\cdot p_j, m_e^2, m_f^2) = \frac{1}{\Gamma\left(3-\frac{D}{2}\right)\pi^{(D-4)/2}}\frac{m_f^{D-4}}{4\pi^2}\int^{\omega}\frac{d^Dk}{k_0}\frac{1}{(p_1\cdot k)(p_j\cdot k)}\,. \tag{70}$$

The calculation of the integrals I_{1j} follows the procedure outlined in [54] and is described in detail in Appendix A of [36]. We need only the leading terms of the small electron mass expansion of these integrals, which to $\mathcal{O}\left((D-4)^0\right)$ read

$$I_{11} = \frac{1}{2m_e^2}\left[\frac{2}{D-4} + \ln\left(\frac{4\omega^2}{s}\right) + \ln\left(\frac{s}{m_f^2}\right) - \ln\left(\frac{s}{m_e^2}\right)\right] + \mathcal{O}\left(m_e^0\right)\,, \tag{71}$$

$$I_{12} = \frac{1}{s}\left[\ln\left(\frac{s}{m_e^2}\right)\left(\frac{2}{D-4} + \ln\left(\frac{4\omega^2}{s}\right) + \ln\left(\frac{s}{m_f^2}\right)\right) - \frac{1}{2}\ln^2\left(\frac{s}{m_e^2}\right) - 2\zeta(2)\right] + \mathcal{O}\left(\frac{m_e^2}{s}\right)\,, \tag{72}$$

$$I_{13} = \frac{1}{t}\left[\ln\left(-\frac{t}{m_e^2}\right)\left(\frac{2}{D-4} + \ln\left(\frac{4\omega^2}{s}\right) + \ln\left(\frac{s}{m_f^2}\right)\right) - \frac{1}{2}\ln^2\left(\frac{s}{m_e^2}\right) - \mathrm{Li}_2\left(1+\frac{s}{t}\right) - 2\zeta(2)\right] + \mathcal{O}\left(\frac{m_e^2}{t}\right)\,, \tag{73}$$

$$I_{14} = \frac{1}{u}\left[\ln\left(-\frac{u}{m_e^2}\right)\left(\frac{2}{D-4} + \ln\left(\frac{4\omega^2}{s}\right) + \ln\left(\frac{s}{m_f^2}\right)\right) - \frac{1}{2}\ln^2\left(\frac{s}{m_e^2}\right) - \mathrm{Li}_2\left(1+\frac{s}{u}\right) - 2\zeta(2)\right] + \mathcal{O}\left(\frac{m_e^2}{u}\right)\,. \tag{74}$$

Note that the term proportional to $(D-4)$ in Eq. (66) gives a finite contribution to Eq. (68), since J_{1j} contain an infrared pole.

6 Numerical Analysis

In this Section we consider the application of our result to the phenomenologically interesting cases relevant for physics at DAΦNE and the ILC. We provide a detailed account of the pure QED contribution, extend the analysis to the mixed QED-QCD corrections, and give an estimate of the hadronic vacuum polarization effect. All the terms involving the logarithm of the IR cut-off ω, $\ln(4\omega^2/s)$, are excluded from the numerical estimates because the corresponding

$\sqrt{s} = 1$ GeV

θ	e (10^{-4})	μ (10^{-4})	c (10^{-4})	τ (10^{-4})	b (10^{-4})
50°	17.341004	1.7972877	0.0622677	0.0264013	0.0010328
60°	18.407836	2.2267654	0.0861876	0.0367058	0.0014184
70°	19.438718	2.6504950	0.1086126	0.0465329	0.0018907
80°	20.465455	3.0655973	0.1253094	0.0540991	0.0022442
90°	21.463240	3.4581845	0.1321857	0.0576348	0.0024428
100°	22.366427	3.8070041	0.1268594	0.0560581	0.0024304
110°	23.099679	4.0922189	0.1098317	0.0495028	0.0022024
120°	23.605216	4.3030725	0.0843311	0.0392810	0.0018086
130°	23.847394	4.4392717	0.0549436	0.0273145	0.0013297

Table 1: *The second-order electron, muon, c-quark, τ-lepton, and b-quark QED contributions to the differential cross section of Bhabha scattering at $\sqrt{s} = 1$ GeV in units of 10^{-4} of the Born cross section.*

contribution critically depends on the event selection algorithm and cannot be unambiguously estimated without imposing specific cuts on the photon bremsstrahlung. The actual impact of the two-loop virtual corrections on the theoretical predictions can be determined only after the result of the paper is consistently implemented into the Monte-Carlo event generators. Nevertheless, the above naïve procedure can be used to get a rough estimate of the magnitude and the structure of the corrections.

As a first application, we consider the Bhabha scattering at $\sqrt{s} = 1$ GeV. The latter is the value of the center-of-mass energy of the KLOE experiment at DAΦNE, which plays a crucial role in the determination of the hadronic vacuum polarization contribution to the muon anomalous magnetic moment [10,11]. The anatomy of the heavy-flavor two-loop correction for this choice of the center-of-mass energy is shown in Fig. 7, where the case in which the heavy fermion is the τ-lepton is considered. Each curve plotted in Fig. 7 represents a specific subset of the virtual corrections and the corresponding soft emission. The dominant contribution originates from the two-loop reducible corrections and from the product of the one-loop corrections, which are considered together (see Sections 5.4 and 5.5). This subset is numerically dominant because it contains all the large collinear logarithms $\ln(s/m_e^2)$. The numerical values of the ratio of the second-order heavy-flavor corrections to the Born QED cross section (Eq. (6)) are collected in Table 1.[11] We separately consider the contributions of muon, τ-lepton, c-quark and b-quark. Since at KLOE one is particularly interested in the large angle scattering events, we considered the angular range between 50 and 130 degrees. For comparison we also give the value of the electron vacuum polarization contribution.[12] The following input parameters are used: $m_e = 0.510998902$ MeV, $m_\mu = 0.105658369$ GeV, $m_\tau = 1.7$ GeV, $m_c = 1.25$ GeV, and $m_b = 4.7$ GeV. The contributions of the τ-lepton, c- and b-quark are suppressed with respect to the muon at least by one order of magnitude. The total heavy-flavor contribution is dominated by the muon loop and it reaches 0.45 permille in magnitude at $\theta \sim 140°$. Note that the energy

[11] Note that the numerical evaluation of our analytic formulas is done with double Fortran precision but we do not present here all the available significant digits

[12] The electron contribution includes the logarithmic part of the soft-pair production. The logarithms of the soft-pair cut-off are excluded from the numerical estimates [25].

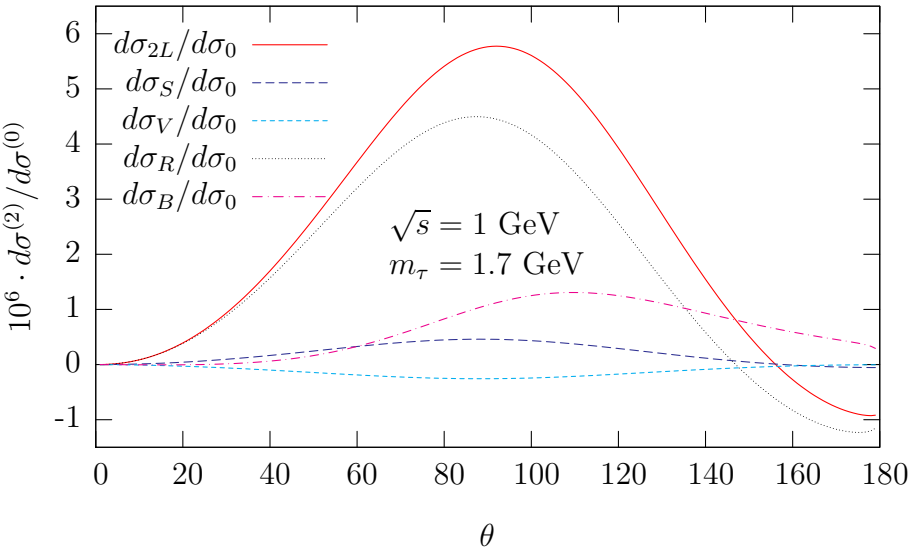

Figure 7: *Self-energy ("S"), vertex ("V"), reducible plus one-loop times one-loop ("R"), and box ("B") contributions to the two-loop τ-lepton correction to the differential cross section of Bhabha scattering at $\sqrt{s} = 1$ GeV.*

under consideration is sufficiently below the quarkonium threshold so that $\sqrt{4m_f^2 - s} \gg \Lambda_{QCD}$ and the heavy quarks can be treated perturbatively. Moreover, for the heavy-quark vacuum polarization in two-loop approximation one has to take into account the first order corrections in the strong coupling constant α_s due to a gluon exchange inside the quark loop. The resulting $\mathcal{O}(\alpha\alpha_s)$ correction to the Bhabha cross section can be obtained from the QED contribution, Eq. (43), by adjusting the overall factor:

$$\frac{d\sigma_2^V}{d\Omega}\Big|^{QCD}_{(2l,S)} = \frac{C_F}{Q_f^2}\,\frac{\alpha_s(m_f^2)}{\alpha}\,\frac{d\sigma_2^V}{d\Omega}\Big|_{(2l,S)} . \tag{75}$$

$C_F = (N_c^2 - 1)/(2N_c)$ is the Casimir operator of the fundamental representation of the $SU(N_c)$ color group, and the strong coupling constant is evaluated at the scale $\mu = m_f$, using the NLO RG equation with the appropriate number of active quarks, starting from the input value $\alpha_S(M_Z) = 0.118$. The numerical results for the $\mathcal{O}(\alpha\alpha_s)$ corrections are listed in the first and the second columns in Table 2. At the same time, the contribution of the light u-, d-, and s-quark to the vacuum polarization is non-perturbative, due to the hadronization effects. In principle, it requires a special treatment based on the integration of the experimentally measured spectral density within the dispersion relation method (see *e.g.* [55]), as it was done in [47]. However, this contribution can be estimated by naïve use of the perturbative result with effective light quark masses. Such estimates are normally in good agreement with the result of the rigorous analysis. To estimate the hadronic contribution at two-loop level we use, for the three light quarks u, d and s, the value $m_u = m_d = m_s = m_{eff} \sim 180$ MeV adopted to describe in the lowest order the hadronic contribution to the muon anomalous magnetic moment [56]. The numerical results for the light-quark contribution at KLOE energies are included in the third column of Table 2. It is comparable to the contribution of the muon (*c.f.* Table 1). Note that

$\sqrt{s} = 1$ GeV	b (10^{-4})	c (10^{-4})	$u+s+d$ (10^{-4})
50°	0.0040026	0.3605297	1.8
60°	0.0053684	0.4787401	2.4
70°	0.0065839	0.5795114	3.0
80°	0.0074290	0.6427167	3.6
90°	0.0077240	0.6528096	4.2
100°	0.0073994	0.6051311	4.7
110°	0.0065277	0.5082196	5.1
120°	0.0052908	0.3802358	5.4
130°	0.0039094	0.2421310	5.6

Table 2: *The second-order $\mathcal{O}(\alpha\alpha_s)$ contribution of b and c quarks, and the light-quark (hadronic) contribution to the differential cross section of Bhabha scattering at $\sqrt{s} = 1$ GeV in units of 10^{-4} of the Born cross section.*

at $\theta = 90^\circ$ our estimate reproduces the value given in [47] with 20% accuracy, sufficient for phenomenological applications at DAΦNE.

Let us now discuss Bhabha scattering at high energies, characteristic to the ILC. We consider two cases: the Giga-Z option with $\sqrt{s} = M_Z$,[13] and $\sqrt{s} = 500$ GeV. In the first case, we consider the contributions of the leptons and the top quark perturbatively and give an estimate of the non-perturbative hadronic contribution due to the five "light" quarks, u, d, s, c and b, using the effective quark mass approach. We use the following values for the effective masses: $m_u = m_d = m_s = m_{eff} \sim 66$ MeV, $m_c = 1.25$ GeV, and $m_b = 4.7$ GeV. These values were adopted to describe the lowest order contribution to $\alpha(M_Z)$ [57]. The numerical results are collected in Table 3. The hadronic contribution is of the same size as the electron vacuum polarization contribution and exceeds the one of the muon. Note that our estimate reproduces the result of [47] at the scattering angles 90° and 3° with 25% and 10% accuracy, respectively. For the small angle scattering, which is of primary interest, our result provides the necessary accuracy of 0.1 permille.

For $\sqrt{s} = 500$ GeV, we consider only the contributions of the leptons and the top quark. The large electroweak decay width of the top quark serves as an infrared regulator and it suppresses the hadronization effects. Therefore, the perturbative result is applicable at energies near and above the top-antitop threshold. At the same time, the effective mass approach for the contribution of lighter quarks is not reliable at this energy. The corrections become sizable due to the logarithmically growing terms and and a rough estimate with an error of about 25%, is not accurate enough to match the luminosity precision requirements. Different subsets of the second order correction due to the top-quark vacuum polarization to the Bhabha scattering cross section are plotted separately in Fig. 8. In this figure we include also the $\mathcal{O}(\alpha\alpha_s)$ corrections to the cross section described by the term in Eq. (75). The numerical results for the two-loop corrections due to electron, muon, τ-lepton, and top quark vacuum polarizations for a center-of-mass energy of $\sqrt{s} = 500$ GeV are collected in Table 4. Note that the contribution of muon and τ-lepton can be significantly reduced if one takes into account the corresponding soft pair emission, which is justified at this energy from an experimental point of view.

[13]The consideration we make about Giga-Z are valid for LEP1 as well.

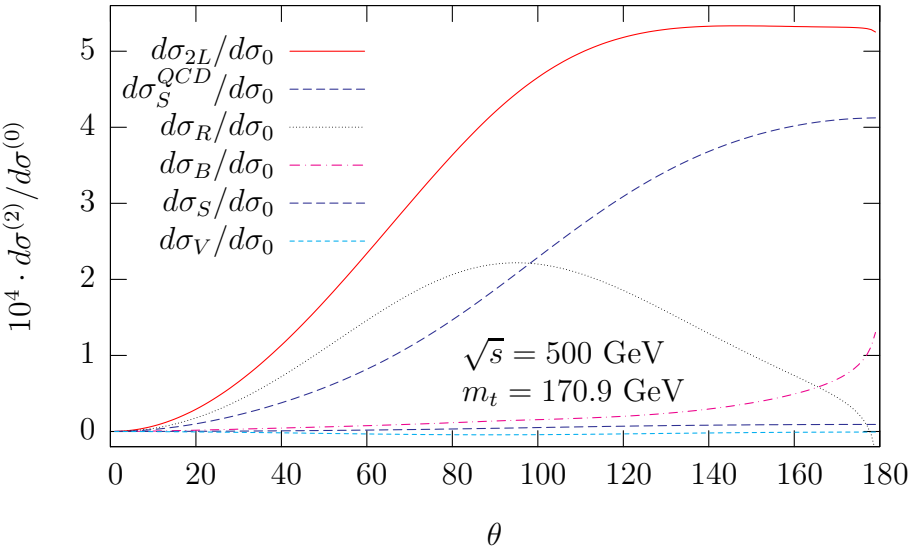

Figure 8: *QED and QCD self-energy ("S"), vertex ("V"), reducible plus one-loop times one-loop ("R") and box ("B") contribution to the two-loop top-quark corrections to the differential cross section of Bhabha scattering at* $\sqrt{s} = 500$ *GeV.*

$\sqrt{s} = m_Z$

θ	e (10^{-3})	μ (10^{-3})	τ (10^{-3})	t (10^{-3})	$b+c+s+d+u$ (10^{-3})
1°	2.1829158	0.3571385	0.0064077	0.0000043	0.93
2°	2.6802340	0.5863583	0.0265766	0.0000151	1.4
3°	2.9952706	0.7349688	0.0573071	0.0000348	1.8
50°	5.5606265	1.7801664	0.9801997	0.0099775	5.2
60°	5.7514057	1.8360794	1.0669528	0.0134970	5.5
70°	5.9332685	1.8891102	1.1471133	0.0166760	5.7
80°	6.1126124	1.9410784	1.2228401	0.0189268	5.9
90°	6.2857772	1.9882767	1.2925934	0.0197396	6.1
100°	6.4419768	2.0231625	1.3524844	0.0188814	6.2
110°	6.5686702	2.0374326	1.3983882	0.0165063	6.3
120°	6.6561657	2.0245734	1.4276615	0.0130914	6.3
130°	6.6983373	1.9800878	1.4394412	0.0092460	6.2

Table 3: *The second-order electron, muon,* τ*-lepton, top-quark, and light-quark contributions to the Bhabha scattering differential cross section for the Giga-Z option of the ILC and LEP1 center-of-mass energy* $\sqrt{s} = M_Z$*. The numbers are given in units of* 10^{-3} *of the Born cross section. The top-quark contribution includes the* $\mathcal{O}(\alpha\alpha_s)$ *term.*

$\sqrt{s} = 500$ GeV

θ	e (10^{-3})	μ (10^{-3})	τ (10^{-3})	t (10^{-3})
1°	3.4957072	0.9690710	0.1542329	0.0000575
2°	4.1203687	1.2491270	0.3573661	0.0002466
3°	4.5099086	1.4146106	0.5140242	0.0005763
50°	7.5740980	2.3185800	1.8411736	0.1707137
60°	7.7965875	2.3446744	1.9274750	0.2340996
70°	8.0081541	2.3708714	2.0072240	0.2998535
80°	8.2164081	2.3981523	2.0829886	0.3635031
90°	8.4172449	2.4207950	2.1521199	0.4202418
100°	8.5982864	2.4282953	2.2085332	0.4655025
110°	8.7451035	2.4090920	2.2456055	0.4979010
120°	8.8465287	2.3536259	2.2585305	0.5181602
130°	8.8954702	2.2543834	2.2446158	0.5287459

Table 4: *The second-order electron, muon, τ-lepton, and top-quark contributions to the differential cross section of Bhabha scattering at $\sqrt{s} = 500$ GeV in units of 10^{-3} of the Born cross section. The top-quark contribution includes the $\mathcal{O}(\alpha\alpha_s)$ term.*

7 Conclusions

In the present work we derived the two-loop radiative corrections to Bhabha scattering due to the vacuum polarization by the virtual heavy-flavor fermion-antifermion pairs. This completes the QED analysis of the process at the two-loop level. The result is valid for arbitrary ratio of the Mandelstam invariants to the heavy fermion mass, provided all these quantities are large compared to the electron mass. The corrections to the cross section are expressed in terms of ordinary harmonic polylogarithms and Nielsen polylogarithms of ratios of polynomials in s and t invariants. Thus we have complete control over its analytic properties and numerical evaluation. The analytical result for the total two-loop QED corrections, which includes also the photonic and the electron vacuum polarization contributions [24,35,36], is now available [59].

We suggested a new approach which reduces the number of mass scales in the most complicated part of the calculation. The approach is based on the general properties of the infrared and collinear divergencies and could be useful for the high-order perturbative calculations in a wide class of processes with a clear mass hierarchy.

The numerical impact of the perturbative second-order heavy-flavor corrections, including the $\mathcal{O}(\alpha\alpha_s)$ contribution for heavy quarks, was studied for the KLOE experiment at DAΦNE as well as for the GigaZ and the high-energy options of the ILC. For the first two applications we also provided an estimate of the hadronic vacuum polarization contribution.

Our result is crucial for the high-precision physics at electron-positron colliders. It removes the last piece of pure theoretical uncertainty in luminosity determination at the low-energy accelerators and gives the proper account for the top quark effects at the ILC. The accuracy of the luminosity determination at low-energy accelerators is now restricted only by the precision of the Monte-Carlo event generators for the hard photon and electron-positron pair emission. To achieve such an accuracy for the large angle scattering at the ILC one has to perform

more careful analysis of the hadronic contribution [47] and take into account also yet unknown two-loop electroweak corrections.[14]

Acknowledgements

We are grateful to J. Vermaseren and D. Maitre for their kind assistance in the use of `FORM` [60], and of the `Mathematica` packages `HPL` and HypExp [42,61]. R. B. would like to thank D. Greynat for useful discussions about Mellin-Barnes [62], the Galileo Galilei Institute for Theoretical Physics for the hospitality and the INFN for partial support. The work of R. B. was partially supported by Ministerio de Educación y Ciencia (MEC) under grant FPA2004-00996, Generalitat Valenciana under grant GVACOMP2007-156, European Commission under the grant MRTN-CT-2006-035482 (FLAVIAnet), and MEC-INFN agreement. The work of A. F. was supported by the Swiss National Science Foundation (SNF) under contract 200020-117602.

A Generalized Harmonic Polylogarithms

For $m_e = 0$ the two-loop corrections are function of s, t, u, and m_f. It is convenient to use the dimensionless variables x and y given by Eq. (19), and $z = R^2/m_f^2 = -u/m_f^2$. To make the formulas as compact as possible we introduce six *rescaled* dimensionless quantities. In particular, in the non physical region $s < 0$, we define:

$$x_r = \frac{\sqrt{P^2+4m_f^2}-\sqrt{P^2}}{\sqrt{P^2+4m_f^2}+\sqrt{P^2}}, \quad \frac{s}{m_f^2} = -\frac{(1-x_r)^2}{x_r}, \tag{76}$$

$$y_r = \frac{\sqrt{Q^2+4m_f^2}-\sqrt{Q^2}}{\sqrt{Q^2+4m_f^2}+\sqrt{Q^2}}, \quad \frac{t}{m_f^2} = -\frac{(1-y_r)^2}{y_r}, \tag{77}$$

$$z_r = \frac{\sqrt{R^2+4m_f^2}-\sqrt{R^2}}{\sqrt{R^2+4m_f^2}+\sqrt{R^2}}, \quad \frac{u}{m_f^2} = -\frac{(1-z_r)^2}{z_r}, \tag{78}$$

$$x_b = \frac{\sqrt{P^2}-\sqrt{P^2-4m_f^2}}{\sqrt{P^2}+\sqrt{P^2-4m_f^2}}, \quad \frac{s}{m_f^2} = -\frac{(1+x_b)^2}{x_b}, \tag{79}$$

$$y_b = \frac{\sqrt{Q^2}-\sqrt{Q^2-4m_f^2}}{\sqrt{Q^2}+\sqrt{Q^2-4m_f^2}}, \quad \frac{t}{m_f^2} = -\frac{(1+y_b)^2}{y_b}, \tag{80}$$

$$z_b = \frac{\sqrt{R^2}-\sqrt{R^2-4m_f^2}}{\sqrt{R^2}+\sqrt{R^2-4m_f^2}}, \quad \frac{u}{m_f^2} = -\frac{(1+z_b)^2}{z_b}. \tag{81}$$

[14] In the case of $e^+e^- \to \mu^+\mu^-$ annihilation the two-loop electroweak corrections enhanced by powers of the large logarithm $\ln(M_{W,Z}^2/s)$, which are dominant for $\sqrt{s}\gtrsim$500 GeV, were computed in [58]. This analysis can be generalized to the Bhabha scattering by adding the t-channel contribution.

The rescaled variable y_r is positive for $y > 0$, while the rescaled variable y_b is positive for $y > 4$ and is a pure phase for $0 < y < 4$. These properties hold also for the variables $z,\ z_r,\ z_b$ and $x,\ x_r,\ x_b$. The analytical result for the cross section can be expressed in terms of a suitable set of GHPLs depending on two of the three variables $x,\ y$, and z. Let us consider the pair of variables x and y. In this case the set of the weight functions is:

$$f_0(x) = \frac{1}{x}\,, \qquad f_{-\mu}(x) = \frac{1}{\sqrt{x(4+x)}}\,, \qquad f_{\mu}(x) = \frac{1}{\sqrt{x(4-x)}}\,,$$
$$f_{-y}(x) = \frac{1}{x+y}\,, \quad f_{-4}(x) = \frac{1}{x+4}\,, \qquad f_{-y-\mu}(x) = \frac{1}{(x+y)\sqrt{x(4+x)}}\,. \tag{82}$$

The GHPLs of weight one are defined as follows:

$$G(0;x) = \ln(x)\,, \quad G(a;x) = \int_0^x dt f_a(t)\,; \tag{83}$$

while GHPLs of higher weight are defined by the iterated integration

$$G(a,\cdots;x) = \int_0^x dt f_a(t) G(\cdots;t)\,, \tag{84}$$

with the only exception of the weight zero GHPLs, which are defined as follows:

$$G(\underbrace{0,\cdots,0}_{n};x) = \frac{1}{n!}\ln^n(x)\,. \tag{85}$$

The GHPLs defined in this way satisfy the usual shuffle algebra [40]. The subset of GHPLs which do not involve the weights $-y$ and $-y-\mu$ can be expressed in terms of the ordinary harmonic polylogarithms (HPLs) of the arguments x_r or y_r, and weights 1, 0, and -1. The table of transformations useful for our calculation reads

$$\begin{aligned}
G(0;y) &= -H(0;y_r) - 2H(1;y_r)\,, && (86)\\
G(-\mu;y) &= -H(0;y_r)\,, && (87)\\
G(-4;y) &= -2\ln(2) + 2H(-1;y_r) - H(0;y_r)\,, && (88)\\
G(0,0;y) &= H(0,0;y_r) + 2H(0,1;y_r) + 2H(1,0;y_r) + 4H(1,1;y_r)\,, && (89)\\
G(-\mu,-\mu;y) &= H(0,0;y_r)\,, && (90)\\
G(-4,-\mu;y) &= -\zeta(2) - 2H(-1,0;y_r) + H(0,0;y_r)\,, && (91)\\
G(-\mu,-4;y) &= \zeta(2) + 2\ln(2)H(0;y_r) - 2H(0,-1;y_r) + H(0,0;y_r)\,, && (92)\\
G(-4,-4;y) &= 2\ln^2(2) - 4\ln(2)H(-1;y_r) + 4H(-1,-1;y_r) - 2H(-1,0;y_r)\\
&\quad +2\ln(2)H(0;y_r) - 2H(0,-1;y_r) + H(0,0;y_r)\,, && (93)\\
G(0,-\mu;y) &= 2\zeta(2) + H(0,0;y_r) + 2H(1,0;y_r)\,, && (94)\\
G(0,0,0;y) &= -H(0,0,0;y_r) - 2H(0,0,1;y_r) - 2H(0,1,0;y_r) - 4H(0,1,1;y_r)\\
&\quad -2H(1,0,0;y_r) - 4H(1,0,1;y_r) - 4H(1,1,0;y_r)\\
&\quad -8H(1,1,1;y_r)\,, && (95)\\
G(-\mu,-\mu,-\mu;y) &= -H(0,0,0;y_r)\,, && (96)
\end{aligned}$$

$$
\begin{aligned}
G(-\mu,-4,-\mu;y) &= 3\zeta(3)+\zeta(2)H(0;y_r)+2H(0,-1,0;y_r)-H(0,0,0;y_r)\,, && (97)\\
G(-4,-4,-\mu;y) &= 2\zeta(3)-2\zeta(2)H(-1;y_r)-4H(-1,-1,0;y_r)+2H(-1,0,0;y_r)\\
&\quad +\zeta(2)H(0;y_r)+2H(0,-1,0;y_r)-H(0,0,0;y_r)\,, && (98)\\
G(0,0,-\mu;y) &= 2\zeta(3)-2\zeta(2)H(0;y_r)-H(0,0,0;y_r)-2H(0,1,0;y_r)\\
&\quad -4\zeta(2)H(1;y_r)-2H(1,0,0;y_r)-4H(1,1,0;y_r)\,, && (99)\\
G(-\mu,0,-\mu;y) &= -4\zeta(3)-2\zeta(2)H(0;y_r)-H(0,0,0;y_r)-2H(0,1,0;y_r)\,, && (100)\\
G(0,-\mu,-\mu;y) &= 2\zeta(3)-H(0,0,0;y_r)-2H(1,0,0;y_r)\,, && (101)\\
G(-4,-\mu,-\mu;y) &= -\frac{3}{2}\zeta(3)+2H(-1,0,0;y_r)-H(0,0,0;y_r)\,, && (102)\\
G(0;x) &= 2H(-1;x_b)-H(0;x_b)\,, && (103)\\
G(\mu;x) &= \pi+iH(0;x_b)\,, && (104)\\
G(0,0;x) &= 4H(-1,-1;x_b)-2H(-1,0;x_b)-2H(0,-1;x_b)+H(0,0;x_b)\,, && (105)\\
G(\mu,\mu;x) &= -3\zeta(2)-H(0,0;x_b)\,, && (106)\\
G(\mu,0;x) &= -i\zeta(2)+2iH(0,-1;x_b)-iH(0,0;x_b)\,, && (107)\\
G(0,0,0;x) &= 8H(-1,-1,-1;x_b)-4H(-1,-1,0;x_b)-4H(-1,0,-1;x_b)\\
&\quad +2H(-1,0,0;x_b)-4H(0,-1,-1;x_b)+2H(0,-1,0;x_b)\\
&\quad +2H(0,0,-1;x_b)-H(0,0,0;x_b)\,, && (108)\\
G(\mu,\mu,0;x) &= -2\zeta(3)+\zeta(2)H(0;x_b)-2H(0,0,-1;x_b)+H(0,0,0;x_b)\,. && (109)
\end{aligned}
$$

The auxiliary two-loop box B-functions listed in Appendix B involve three GHPLs which depend on two different kinematical variables. These GHPLs can be expressed in terms of the logarithms and Nielsen's polylogarithms depending on the rescaled variables:

$$
\begin{aligned}
G(-x-\mu;y) &= \int_0^y dw\frac{1}{(w+x)\sqrt{w(4+w)}}\,,\\
&= -\frac{x_b}{(1-x_b)(x_b+1)}\left(\ln(x_b+y_r)-\ln(x_by_r+1)\right)\,, && (110)\\
G(-x,-\mu;y) &= \int_0^y dw\frac{1}{w+x}\int_0^w dr\frac{1}{\sqrt{r(4+r)}}\,,\\
&= \ln^2(y_r)-\ln(x_b+y_r)\ln(y_r)-\ln(x_by_r+1)\ln(y_r)+\mathrm{Li}_2\left(-\frac{x_b}{y_r}\right)\\
&\quad -\mathrm{Li}_2(-x_by_r)\,, && (111)\\
G(-x,0,-\mu;y) &= \int_0^y dw\frac{1}{w+x}\int_0^w dq\frac{1}{q}\int_0^q dr\frac{1}{\sqrt{r(4+r)}}\,,\\
&= \ln(1+x_b)\Big\{-2\ln(y_r)[\ln(x_by_r+1)+\ln(x_b+y_r)-\ln(y_r)]-8\zeta(2)\\
&\quad -2\mathrm{Li}_2\left(\frac{x_by_r+1}{x_by_r}\right)-2\mathrm{Li}_2\left(\frac{x_b+y_r}{y_r}\right)-2\mathrm{Li}_2\left(\frac{x_by_r+1}{1+x_b}\right)-2\mathrm{Li}_2\left(\frac{x_b+y_r}{1+x_b}\right)\\
&\quad +2\mathrm{Li}_2\left(\frac{x_by_r+1}{y_r(1+x_b)}\right)+2\mathrm{Li}_2\left(\frac{x_b+y_r}{y_r(1+x_b)}\right)-2\ln(x_b)\ln(y_r)+4\ln(y_r)\ln(1-y_r)\\
&\quad +4\mathrm{Li}_2(1-y_r)+8\mathrm{Li}_2(y_r)+4\ln^2(1+x_b)\ln(y_r)\Big\}+[\ln(x_b+y_r)-\ln(y_r)]\Big[2\zeta(2)
\end{aligned}
$$

$$
\begin{aligned}
&+2\mathrm{Li}_2\left(\frac{x_b+y_r}{y_r}\right)+2\mathrm{Li}_2\left(\frac{x_b+y_r}{1+x_b}\right)-2\mathrm{Li}_2\left(\frac{x_b+y_r}{y_r(1+x_b)}\right)-2\mathrm{Li}_2(y_r)\Big]\\
&+\ln(x_by_r+1)\Big[2\zeta(2)+2\mathrm{Li}_2\left(\frac{x_by_r+1}{x_by_r}\right)+2\mathrm{Li}_2\left(\frac{x_by_r+1}{1+x_b}\right)-2\mathrm{Li}_2\left(\frac{x_by_r+1}{y_r(1+x_b)}\right)\\
&+2\ln(x_b)\ln(y_r)+\frac{1}{2}\ln^2(y_r)-2\mathrm{Li}_2(y_r)\Big]-2\mathrm{Li}_3\left(\frac{x_by_r+1}{x_by_r}\right)-2\mathrm{Li}_3\left(\frac{x_b+y_r}{y_r}\right)\\
&-2\mathrm{Li}_3\left(\frac{x_by_r+1}{1+x_b}\right)-2\mathrm{Li}_3\left(\frac{x_b+y_r}{1+x_b}\right)+2\mathrm{Li}_3\left(\frac{x_by_r+1}{y_r(1+x_b)}\right)+2\mathrm{Li}_3\left(\frac{x_b+y_r}{y_r(1+x_b)}\right)\\
&-\ln(y_r)\Big[2\mathrm{Li}_2\left(\frac{x_by_r+1}{x_by_r}\right)-2\mathrm{Li}_2\left(\frac{x_b+y_r}{1+x_b}\right)-2\mathrm{Li}_2\left(\frac{x_by_r+1}{y_r(1+x_b)}\right)-\mathrm{Li}_2\left(-\frac{y_r}{x_b}\right)\\
&-\mathrm{Li}_2(-x_by_r)\Big]+\frac{1}{6}\ln^2(y_r)[3\ln(x_b+y_r)-4\ln(y_r)-6\ln(x_b)]+2\mathrm{Li}_3\left(\frac{1+x_b}{x_b}\right)\\
&+2\mathrm{Li}_3(1+x_b)-\mathrm{Li}_3\left(-\frac{y_r}{x_b}\right)+\mathrm{Li}_3\left(-\frac{1}{x_b}\right)-\mathrm{Li}_3(-x_by_r)+\mathrm{Li}_3(-x_b)\,, \qquad (112)
\end{aligned}
$$

where the Nielsen's polylogarithms are related to HPLs as follows:

$$
\mathrm{Li}_n(a)=H(\underbrace{0,\cdots,0}_{n},1;a)\,,\quad \mathrm{S}_{n,m}(a)=H(\underbrace{0,\cdots,0}_{n},\underbrace{1,\cdots,1}_{m};a)\,. \qquad (113)
$$

A.1 Analytical Continuation

The result for the two-loop corrections in Section 5 is expressed in terms of the auxiliary functions which are given in Appendix B in the non-physical region $s<0$. The corresponding expressions in the physical region $s>0$ can be obtained by analytical continuation to the complex value of P^2:

$$
P^2=-s-i\epsilon,\qquad \epsilon\to 0^+\,. \qquad (114)
$$

Not that in the physical region Q^2 and R^2 are real and positive. Let us consider the analytical structure of the rescaled variables, Eqs. (76–81). The variables y_r and z_r are positive and vary from 0 to 1 for $0<Q^2<\infty$ and $0<R^2<\infty$. The variable x_r varies from 0 to 1 for $0<P^2<\infty$. For positive s the variable x_r becomes complex. In the region $0<s<4m_f^2$ it is a pure phase:

$$
x_r=\frac{\sqrt{4m_f^2-s}+i\sqrt{s}}{\sqrt{4m_f^2-s}-i\sqrt{s}}=e^{i2\phi}\,, \qquad (115)
$$

where

$$
\phi=\arctan\sqrt{\frac{s}{4m_f^2-s}}\,. \qquad (116)
$$

In the region $s>4m_f^2$ we have

$$
x_r=-x_r'+i\epsilon\,, \qquad (117)
$$

with

$$
x_r'=\frac{\sqrt{s}-\sqrt{s-4m_f^2}}{\sqrt{s}+\sqrt{s-4m_f^2}}\,. \qquad (118)
$$

The HPLs of the variables y_r and z_r are always real, while the HPLs of x_r are complex for $s > 0$. In particular, their imaginary part in the region above the heavy-flavor threshold, $s > 4m_f^2$, is defined when the analytical continuation of the logarithm is specified:

$$H(0; x_r) \to H(0; -x'_r + i\epsilon) = H(0; x'_r) + i\pi \,. \tag{119}$$

The case of the variables x_b, y_b, and z_b is more complicated. The variables y_b and z_b can be complex. For $0 < Q^2, R^2 < 4m_f^2$, y_b and z_b are pure phases. Note that the expressions of t and u in terms of y_b and z_b are invariant under the inversion

$$y_b \to \frac{1}{y_b} \,, \qquad z_b \to \frac{1}{z_b} \,. \tag{120}$$

This means that for $0 < Q^2, R^2 < 4m_f^2$ it does not matter whether we give to Q^2 and R^2 a positive or a negative imaginary part. Let us choose $Q^2 \to Q^2 - i\epsilon$ and $R^2 \to R^2 - i\epsilon$. Then we have

$$y_b = \frac{\sqrt{Q^2} + i\sqrt{4m_f^2 - Q^2}}{\sqrt{Q^2} - i\sqrt{4m_f^2 - Q^2}} = e^{i2\psi} \,, \tag{121}$$

$$z_b = \frac{\sqrt{R^2} + i\sqrt{4m_f^2 - R^2}}{\sqrt{R^2} - i\sqrt{4m_f^2 - R^2}} = e^{i2\xi} \,, \tag{122}$$

with

$$\psi = \arctan \sqrt{\frac{4m_f^2}{Q^2} - 1} \,, \tag{123}$$

$$\xi = \arctan \sqrt{\frac{4m_f^2}{R^2} - 1} \,. \tag{124}$$

When Q^2 and R^2 vary from $4m_f^2$ to infinity, y_b and z_b are real and positive and vary from 1 to 0. The variable x_b is a pure phase for $0 < P^2 < 4m_f^2$. It varies from 1 and 0 when P^2 varies from $4m_f^2$ to $+\infty$. In the physical region we have

$$x_b \to -x'_b + i\epsilon \,, \tag{125}$$

where

$$x'_b = \frac{\sqrt{s + 4m_f^2} - \sqrt{s}}{\sqrt{s + 4m_f^2} + \sqrt{s}} \,, \tag{126}$$

i.e. x_b is negative and varies from -1 and 0 when s varies from 0 to ∞. The HPLs of x_b are complex in the physical region. Their imaginary part is defined in the same way as in Eq. (119). Finally, the analytical continuation of the three GHPLs of Eqs. (110–112) are defined by the analytical properties of the functions Li_2 and Li_3 [63].

A.2 Mellin-Barnes Expansion of the GHPLs

To study the low and high energy behavior of the two-loop corrections one needs the expansion of three GHPLs of two kinematical invariants, Eqs. (110-112), in the limits $s \gg m_f^2$ and $s \ll m_f^2$. To perform the expansions we apply the inverse Mellin-Barnes transformation to the integral representation of the GHPLs. In this Section we describe the technique and present the result of the expansion. We start with the GHPL of weight one in Eq. (110):

$$G(-x-\mu;y) \;=\; \int_0^y dw \frac{1}{(w+x)\sqrt{w(4+w)}}\,. \tag{127}$$

By changing the integration variable $w = yr$ we obtain the following integral representation:

$$G(-x-\mu;y) \;=\; \frac{1}{x}\int_0^1 dr \frac{1}{r}\left(1+\frac{y}{x}r\right)^{-1}\left(1+\frac{4}{yr}\right)^{-1/2}\,. \tag{128}$$

Then we apply the inverse Mellin-Barnes transformation to the square root in the integrand:

$$\left(1+\frac{4}{yr}\right)^{-1/2} = \frac{1}{2\pi i}\frac{1}{\Gamma(1/2)}\int_{-i\infty}^{i\infty} d\sigma \Gamma\left(\frac{1}{2}+\sigma\right)\Gamma\left(-\sigma\right)\left(\frac{4}{yr}\right)^{\sigma}\,. \tag{129}$$

The integrand has two infinite series of poles in the σ complex plane:

$$\begin{aligned} &\text{“left hand side poles” at} && \sigma = -n-\frac{1}{2}\,, \quad \text{for} \quad n = 0,1,2,\cdots\,; \\ &\text{“right hand side poles” at} && \sigma = n\,, \quad \text{for} \quad n = 0,1,2,\cdots\,. \end{aligned} \tag{130}$$

One has to choose the integration contour in Eq. (129) so that

$$-\frac{1}{2} < \mathrm{Re}(\sigma) < 0\,. \tag{131}$$

Then we find

$$G(-x-\mu;y) = \frac{1}{2\pi i}\frac{1}{\Gamma(1/2)}\frac{1}{x}\int_{-i\infty}^{i\infty} d\sigma \Gamma\left(\frac{1}{2}+\sigma\right)\Gamma\left(-\sigma\right)\left(\frac{4}{y}\right)^{\sigma} I(\sigma)\,. \tag{132}$$

The integral over r can be evaluated analytically

$$I(\sigma) = \int_0^1 dr r^{-\sigma-1}\left(1+\frac{y}{x}r\right)^{-1} = -\frac{1}{\sigma}\,{}_2\mathrm{F}_1\left(1,-\sigma,1-\sigma;-\frac{y}{x}\right)\,, \tag{133}$$

where ${}_2\mathrm{F}_1$ is the hypergeometric function. In order to obtain the asymptotic expansion in the $y \to \infty$ limit at fixed $\tau = y/x$ it is sufficient to close the integration contour in Eq. (132) on the r.h.s. of the σ complex plane. One finds

$$G(-x-\mu;y) \;=\; \sum_{n=0}^{\infty} g_n^{(1,\mathrm{L})}(\tau,y)\,(1/y)^{n+1}\,, \tag{134}$$

where the functions $g_n^{(1,\mathrm{L})}$ can be easily obtained *e.g.* with the help of [42]. For $n = 0,\ 1,\ 2$ they read

$$g_0^{(1,\mathrm{L})}(\tau,y) = -\tau\left(\ln(\tau+1)-\ln(y)\right), \tag{135}$$

$$g_1^{(1,\mathrm{L})}(\tau,y) = -2\tau\left[\left(\ln(\tau+1)-\ln(y)\right)\tau+\tau-1\right], \tag{136}$$

$$g_2^{(1,\mathrm{L})}(\tau,y) = -\tau\left[6\left(\log(\tau+1)-\log(y)\right)\tau^2+(7\tau-6)\,\tau+3\right]. \tag{137}$$

To obtain the asymptotic expansion of this GHPL in the limit $y \to 0$ for fixed τ it is necessary to close the integration contour in Eq. (132) on the left hand side (l.h.s.) of the σ complex plane. One obtains

$$G(-x-\mu;y) = \sum_{n=0}^{\infty} g_n^{(1,\mathrm{S})}(\tau,y)y^n, \tag{138}$$

where the functions $g_n^{(1,\mathrm{S})}$ for $n = 0,\ 1,\ 2$ read

$$g_0^{(1,\mathrm{S})} = \sqrt{\frac{\tau}{y}}\arctan\left(\sqrt{\tau}\right), \tag{139}$$

$$g_1^{(1,\mathrm{S})} = \frac{\arctan\left(\sqrt{\tau}\right)-\sqrt{\tau}}{8\sqrt{y\tau}}, \tag{140}$$

$$g_2^{(1,\mathrm{S})} = \frac{\sqrt{\tau}(\tau-3)+3\arctan\left(\sqrt{\tau}\right)}{128\sqrt{y\tau^3}}. \tag{141}$$

The expansion of the remaining two GHPLs is almost identical. By inverse Mellin-Barnes transformation the GHPL of weight two in Eq. (111) can be written as

$$\begin{aligned} G(-x,-\mu;y) &= \int_0^y dw\frac{1}{w+x}\int_0^w dr\frac{1}{\sqrt{r(4+r)}} \\ &= \int_0^y dw\frac{1}{w+r}\int_0^1 ds\frac{1}{s}\left(1+\frac{4}{ws}\right)^{-\frac{1}{2}} \\ &= -\frac{1}{2\pi i}\frac{1}{\Gamma(1/2)}\int_{-i\infty}^{i\infty} d\sigma\frac{\Gamma\left(\frac{1}{2}+\sigma\right)\Gamma(-\sigma)}{\sigma}4^\sigma\int_0^y dw\frac{1}{w+x}w^{-\sigma} \\ &= -\frac{1}{2\pi i}\frac{1}{\Gamma(1/2)}\frac{1}{x}\int_{-i\infty}^{i\infty} d\sigma\frac{\Gamma\left(\frac{1}{2}+\sigma\right)\Gamma(-\sigma)}{\sigma(1-\sigma)}4^\sigma y^{1-\sigma}\times \\ &\quad \times{}_2\mathrm{F}_1\left(1,1-\sigma,2-\sigma;-\frac{y}{x}\right). \end{aligned} \tag{142}$$

Again, the integration contour has to satisfy Eq. (131). By closing the integration contour on the r.h.s. of the complex σ plane, in the limit $y \to \infty$ one finds

$$G(-x,-\mu;y) = \sum_{n=0}^{\infty} g_n^{(2,\mathrm{L})}(\tau,y)\,(1/y)^n. \tag{143}$$

The functions $g_n^{(1,\mathrm{L})}$ for $n = 0,\ 1,\ 2$ read

$$g_0^{(2,\mathrm{L})}(\tau,y) = \ln(y)\ln(\tau+1)+\mathrm{Li}_2(-\tau), \tag{144}$$

$$g_1^{(2,\mathrm{L})}(\tau,y) = 2\tau[\ln(y)+\ln(\tau+1)], \tag{145}$$

$$g_2^{(2,\mathrm{L})}(\tau,y) = \tau[3(\ln(y)-\ln(\tau+1))\tau-2\tau+3]. \tag{146}$$

Alternatively, by closing the integration contour on the l.h.s. of the complex σ plane, which corresponds to the limit $y \to 0$, one obtains

$$G(-x,-\mu;y) = \sum_{n=0}^{\infty} g_n^{(2,\mathrm{S})}(\tau,y) y^n \,, \tag{147}$$

with

$$g_0^{(2,\mathrm{S})} = 2\sqrt{\frac{y}{\tau}}\left(\sqrt{\tau} - \arctan\left(\sqrt{\tau}\right)\right) \,, \tag{148}$$

$$g_1^{(2,\mathrm{S})} = -\frac{\sqrt{\frac{y}{\tau}}\left(\sqrt{\tau}(\tau-3)+3\arctan\left(\sqrt{\tau}\right)\right)}{36\tau} \,, \tag{149}$$

$$g_2^{(2,\mathrm{S})} = \frac{\sqrt{\frac{y}{\tau}}\left(\sqrt{\tau}(\tau(3\tau-5)+15)-15\arctan\left(\sqrt{\tau}\right)\right)}{1600\tau^2} \,. \tag{150}$$

For the GHPL of weight three in Eq. (111) we have

$$\begin{aligned} G(-x,0,-\mu;y) &= \int_0^y dw \frac{1}{w+x} \int_0^w dq \frac{1}{q} \int_0^q dr \frac{1}{\sqrt{r(4+r)}} \\ &= \int_0^y dw \frac{1}{w+x} \int_0^w ds \frac{1}{s} \int_0^1 dq \frac{1}{q} \left(1+\frac{4}{sq}\right)^{-\frac{1}{2}} \\ &= \frac{1}{2\pi i} \frac{1}{\Gamma(1/2)} \int_{-i\infty}^{i\infty} d\sigma \Gamma\left(\sigma+\frac{1}{2}\right) \Gamma(-\sigma) 4^\sigma \int_0^y dw \frac{1}{w+x} \times \\ &\quad \times \int_0^w ds\, s^{-\sigma-1} \int_0^1 dq\, q^{-\sigma-1} \\ &= \frac{1}{2\pi i} \frac{1}{\Gamma(1/2)} \frac{1}{x} \int_{-i\infty}^{i\infty} d\sigma \frac{\Gamma\left(\sigma+\frac{1}{2}\right)\Gamma(-\sigma)}{\sigma^2(1-\sigma)} 4^\sigma y^{1-\sigma} \times \\ &\quad \times {}_2\mathrm{F}_1\left(1,1-\sigma,2-\sigma;-\frac{y}{x}\right) \,. \end{aligned} \tag{151}$$

Once again, the condition in Eq. (131) has to be satisfied by the integration contour in Eq. (151). By closing the integration contour on the r. h.s. of the complex σ plane one obtains the asymptotic expansion in the limit $y \to \infty$:

$$G(-x,0,-\mu;y) = \sum_{n=0}^{\infty} g_n^{(3,\mathrm{L})}(\tau,y) \left(1/y\right)^n \,. \tag{152}$$

The first three $g_n^{(3,\mathrm{L})}$ functions are given by

$$g_0^{(3,\mathrm{L})}(\tau,y) = \frac{1}{6}\left(3\ln^2(y)+2\pi^2\right)\ln(\tau+1) + \ln(y)\mathrm{Li}_2(-\tau) - \mathrm{Li}_3(-\tau) \,, \tag{153}$$

$$g_1^{(3,\mathrm{L})}(\tau,y) = -2\tau[\ln(y) - \ln(\tau+1) + 1] \,, \tag{154}$$

$$g_2^{(3,\mathrm{L})}(\tau,y) = -\frac{1}{4}\tau[6(\ln(y)-\ln(\tau+1))\tau - \tau + 6] \,. \tag{155}$$

By closing the integration contour in Eq. (151) on the l.h.s. of the complex σ plane one finds the asymptotic behavior of the GHPL in the $y \to 0$ limit:

$$G(-x, 0, -\mu; y) = \sum_{n=0}^{\infty} g_n^{(3,\mathrm{S})}(\tau, y) y^n \,, \tag{156}$$

where the functions $g_n^{(1,\mathrm{S})}$ for $n = 0, 1, 2$ read

$$g_0^{(3,\mathrm{S})} = 4\sqrt{\frac{y}{\tau}} \left(\sqrt{\tau} - \arctan\left(\sqrt{\tau}\right)\right) \,, \tag{157}$$

$$g_1^{(3,\mathrm{S})} = -\frac{\sqrt{\frac{y}{\tau}} \left(\sqrt{\tau}(\tau - 3) + 3\arctan\left(\sqrt{\tau}\right)\right)}{54\tau} \,, \tag{158}$$

$$g_2^{(3,\mathrm{S})} = \frac{\sqrt{\frac{y}{\tau}} \left(\sqrt{\tau}(\tau(3\tau - 5) + 15) - 15\arctan\left(\sqrt{\tau}\right)\right)}{4000\tau^2} \,. \tag{159}$$

It is interesting that, though the expansion of the three GHPLs discussed above in the $s \ll m_f^2$ limit involves $\arctan(\sqrt{\tau})$ terms, these terms completely cancel in the expansion of the auxiliary functions B_1, B_2, and B_3.

B Auxiliary Functions

In this Appendix we collect the expressions for the auxiliary functions used in the paper which are valid in the non-physical region $s < 0$ ($P^2 > 0$). The analytical continuation to $s > 0$ is discussed in Section A.1. The dimensionless variables x and y, used in the explicit formulas below, are related to s and t via Eq. (19).

B.1 One-Loop Functions

Vacuum polarization:

$$\Pi_0^{(1l)}(s) = \sum_{i=0}^{1} \Pi_0^{(1l,i)}(s)(D-4)^i + \mathcal{O}\left((D-4)^2\right) \,, \tag{160}$$

where:

$$\Pi_0^{(1l,0)} = -\frac{5}{9} + \frac{4}{3x} + \frac{1}{3}\frac{x^2 + 2x - 8}{x\sqrt{x(x+4)}} G(-\mu; x) \,, \tag{161}$$

$$\Pi_0^{(1l,1)} = \frac{14}{27} - \frac{16}{9x} - \frac{1}{18x\sqrt{x(x+4)}} \Big[(4x - 64 + 5x^2) G(-\mu; x) - 3(2x - 8 + x^2) G(-4, -\mu; x) \Big] \,. \tag{162}$$

Dirac form factor:

$$F_1^{(1l)}(s) = \sum_{i=-1}^{0} F_1^{(1l,i)}(s)(D-4)^i + \mathcal{O}(D-4) \,, \tag{163}$$

where:

$$F_1^{(1l,-1)} = 1 - \ln\left(\frac{P^2}{m_e^2}\right), \tag{164}$$

$$F_1^{(1l,0)} = -1 + \frac{1}{2}\zeta(2) - \frac{1}{2}G(0;x) + \left(\frac{5}{4} + \frac{1}{2}G(0;x)\right)\ln\left(\frac{P^2}{m_e^2}\right) - \frac{3}{4}\ln^2\left(\frac{P^2}{m_e^2}\right). \tag{165}$$

Box B-functions:

$$B_j^{(1l)}(s,t) = \sum_{i=-2}^{0} B_j^{(1l,i)}(s,t)(D-4)^i + \mathcal{O}(D-4), \quad j = 1,2,3, \tag{166}$$

where:

$$B_1^{(1l,-2)} = \frac{16(x+y)^2}{y}, \tag{167}$$

$$B_1^{(1l,-1)} = \frac{8(x^2+xy+y^2)}{y} + \frac{8(x+y)^2}{y}G(0;x), \tag{168}$$

$$\begin{aligned} B_1^{(1l,0)} = & -\frac{2(2xy + 8x^2\zeta(2) + 10xy\zeta(2) + 5y^2\zeta(2))}{y} \\ & + \frac{2(2x^2+xy+y^2)}{y}G(0;x) + 2(x+y)G(0;y) + 2(2x+y)G(0,0;x) \\ & + \frac{2(2x^2+2xy+y^2)}{y}\left(G(0;x)G(0;y) - G(0,0;y)\right), \end{aligned} \tag{169}$$

$$B_2^{(1l,-2)} = \frac{16(2x^2+2xy+y^2)}{y}, \tag{170}$$

$$B_2^{(1l,-1)} = 8y + \frac{8(2x^2+2xy+y^2)}{y}G(0;x), \tag{171}$$

$$\begin{aligned} B_2^{(1l,0)} = & -\frac{2(16x^2+10xy+5y^2)\zeta(2)}{y} + \frac{2(4x^2+2xy+y^2)}{y}(G(0;x)G(0;y) - G(0,0;y)) \\ & -2(x-y)G(0;x) + 2(x+y)G(0;y) + 2(2x+y)G(0,0;x), \end{aligned} \tag{172}$$

$$B_3^{(1l,-2)} = -\frac{16x^2}{y}, \tag{173}$$

$$B_3^{(1l,-1)} = -\frac{8(x^2+xy+y^2)}{y} - \frac{8x^2}{y}G(0;x), \tag{174}$$

$$\begin{aligned} B_3^{(1l,0)} = & -\frac{4(xy + y^2 - 4x^2\zeta(2))}{y} - \frac{4x^2}{y}(G(0;x)G(0;y) - G(0,0;y)) \\ & -\frac{4(x^2+xy+y^2)}{y}G(0;x). \end{aligned} \tag{175}$$

B.2 Two-Loop Functions

Vacuum polarization:

$$\Pi_0^{(2l)}(s) = \Pi_0^{(2l,0)}(s) + \mathcal{O}(D-4), \tag{176}$$

where:

$$\begin{aligned}\Pi_0^{(2l,0)} &= \frac{x+4}{12x\sqrt{x(x+4)}}\Big[3(-6+x)G(-\mu;x)+4(2-x)(2G(-4,-\mu;x)+G(0,-\mu;x))\Big]\\ &+\frac{1}{24x^2}\Big[52x-5x^2-8(7-2x-3x^2)G(-\mu,-\mu;x)\\ &+(4-x^2)(16G(-4,-\mu,-\mu;x)+8G(0,-\mu,-\mu;x)-16G(-\mu,-4,-\mu;x)\\ &-8G(-\mu,0,-\mu;x))\Big]\,. \end{aligned} \tag{177}$$

Dirac form factor:

$$F_1^{(2l)}(s) = F_1^{(2l,0)}(s) + \mathcal{O}(D-4)\,, \tag{178}$$

where:

$$\begin{aligned}F_1^{(2l,0)} &= \frac{1}{36x\sqrt{x(4-x)}}[(x-4)(46-19x)G(\mu,0;x)]-\frac{1}{1296x^2}[8568x-3355x^2\\ &-x(3960-1590x)G(0;x)+(1296-216x^2)G(\mu,\mu,0;x)]\,, \end{aligned} \tag{179}$$

Box B-functions:

$$B_j^{(2l)}(s,t) = \sum_{i=-2}^{0} B_j^{(2l,i)}(s,t)(D-4)^i + \mathcal{O}(D-4)\,, \quad j=1,2,3\,, \tag{180}$$

where:

$$B_1^{(2l,-2)} = -\frac{8(x+y)^2(5y-12)}{9y^2}+\frac{8(y-2)(y+4)(x+y)^2}{3y^2\sqrt{y(y+4)}}G(-\mu;y)\,, \tag{181}$$

$$\begin{aligned}B_1^{(2l,-1)} &= -\frac{4(204x^2+444xy-13x^2y+204y^2-41xy^2-13y^3)}{27y^2}\\ &-\frac{8(x+y)^2}{3y}G(-\mu,-\mu;y)-\frac{4(x+y)^2(5y-12)}{9y^2}G(0;x)\\ &-\frac{1}{\sqrt{y(y+4)}}\Big[\frac{4(y+4)(-34x^2-74xy+2x^2y-34y^2+7xy^2+2y^3)}{9y^2}G(-\mu;y)\\ &-\frac{4(y-2)(y+4)(x+y)^2}{3y^2}(3G(-4,-\mu;y)+G(0;x)G(-\mu;y))\Big]\,, \end{aligned} \tag{182}$$

$$\begin{aligned}B_1^{(2l,0)} &= \frac{2(x-4)x(y-2)(y+4)(x+y)^2}{3y^2\sqrt{y(y+4)}\sqrt{x(4-x)}}G(\mu,0;x)G(-x-\mu;y)\\ &+\frac{1}{\sqrt{y(y+4)}}\Big[\frac{2(y-2)(y+4)(x+y)^2}{3y^2}G(-x,0,-\mu;y)\\ &-\frac{4(y-2)(y+4)(x+y)^2}{y^2}G(-\mu,-\mu,-\mu;y)+\frac{y+4}{135y^2}(-1736x^2-4732xy\\ &+82x^2y-1976y^2-16xy^2+9x^2y^2-158y^3+18xy^3+9y^4+180x^2\zeta(2)\\ &+360xy\zeta(2)-90x^2y\zeta(2)+180y^2\zeta(2)-180xy^2\zeta(2)-90y^3\zeta(2))G(-\mu;y)\\ &-\frac{2(y+4)}{3y^2}(-34x^2-74xy+2x^2y-34y^2+7xy^2+2y^3)G(-4,-\mu;y) \end{aligned}$$

$$
\begin{aligned}
&+\frac{2(y-2)(y+4)(x+y)^2}{3y^2}(3G(-4,-\mu;y)G(0;x)+9G(-4,-4,-\mu;y)\\
&-G(0;x)G(-x,-\mu;y))-\frac{4(4+y)}{9y^2}(4x^2+4xy-5x^2y-4y^2-5xy^2-4y^3)G(0,-\mu;y)\\
&-\frac{2(4+y)}{9y^2}(-42x^2-82xy+12x^2y-26y^2+17xy^2+10y^3)G(0;x)G(-\mu;y)\\
&+\frac{2(y-2)(y+4)(x+y)^2}{3y^2}(G(0;x)G(0,-\mu;y)-G(0,0,-\mu;y)+G(0,0;x)G(-\mu;y))\Big]\\
&+\frac{2(x-4)x(12x+20y-5xy+3y^2)}{9y^2\sqrt{x(4-x)}}G(\mu,0;x)-\frac{1}{9y^2}(144x^2+288xy-11x^2y\\
&+144y^2-40xy^2-17y^3)G(-\mu,-\mu;y)-\frac{4(x+y)^2}{y}G(-\mu,-4,-\mu;y)\\
&-\frac{2(2x^2+2xy+y^2)}{3y}G(-\mu,0,-\mu;y)-\frac{2(2x+y)}{3}(G(0;x)G(-\mu,-\mu;y)\\
&+G(\mu,\mu,0;x))+\frac{2(2x^2+6xy+3y^2)}{3y}G(0,-\mu,-\mu;y)+\frac{2}{27y^2}(-180x^2-372xy\\
&+41x^2y-156y^2+121xy^2+65y^3)G(0;x)-\frac{2(x+y)^2(-12+5y)}{9y^2}G(0,0;x)\\
&-\frac{(x+y)^2}{15}G(0;y)+\frac{2}{405y^2}(4488x^2+12036xy-1082x^2y+4488y^2-2359xy^2\\
&-1082y^3-540x^2\zeta(2)-1080xy\zeta(2)+225x^2y\zeta(2)-540y^2\zeta(2)+450xy^2\zeta(2)\\
&+225y^3\zeta(2))\,, \qquad (183)
\end{aligned}
$$

$$
B_2^{(2l,-2)} = \frac{8(2x^2+2xy+y^2)}{9y^2}\left[12-5y+\frac{3(y-2)(y+4)}{\sqrt{y(y+4)}}G(-\mu;y)\right], \qquad (184)
$$

$$
\begin{aligned}
B_2^{(2l,-1)} &= -\frac{4(480x^2+480xy-56x^2y+204y^2-56xy^2-13y^3)}{27y^2}-\frac{4(5y-12)}{9y^2}(2x^2+2xy\\
&+y^2)G(0;x)-\frac{8(2x^2+2xy+y^2)}{3y}G(-\mu,-\mu;y)+\frac{y+4}{\sqrt{y(y+4)}}\Big[\frac{8}{9y^2}(40x^2+40xy\\
&-5x^2y+17y^2-5xy^2-y^3)G(-\mu;y)+\frac{4(y-2)(2x^2+2xy+y^2)}{3y^2}(3G(-4,-\mu;y)\\
&+G(0;x)G(-\mu;y))\Big]\,, \qquad (185)
\end{aligned}
$$

$$
\begin{aligned}
B_2^{(2l,0)} &= \frac{2(x-4)x(y-2)(y+4)(2x^2+2xy+y^2)}{3y^2\sqrt{y(y+4)}\sqrt{x(4-x)}}G(\mu,0;x)G(-x-\mu;y)\\
&+\frac{y+4}{\sqrt{y(y+4)}}\Big[\frac{2(y-2)(2x^2+2xy+y^2)}{3y^2}(G(-x,0,-\mu;y)-6G(-\mu,-\mu,-\mu;y))\\
&-\frac{1}{135y^2}(5872x^2+6112xy-464x^2y+1976y^2-224xy^2-18x^2y^2+158y^3\\
&-18xy^3-9y^4-360x^2\zeta(2)-360xy\zeta(2)+180x^2y\zeta(2)-180y^2\zeta(2)\\
&+180xy^2\zeta(2)+90y^3\zeta(2))G(-\mu;y)+\frac{4}{3y^2}(40x^2+40xy-5x^2y+17y^2-5xy^2
\end{aligned}
$$

$$
\begin{aligned}
&-y^3)G(-4,-\mu;y)+\frac{2(y-2)(2x^2+2xy+y^2)}{3y^2}(3G(-4,-\mu;y)G(0;x)\\
&+9G(-4,-4,-\mu;y)-G(0;x)G(-x,-\mu;y)+G(0;x)G(0,-\mu;y)\\
&-G(0,0,-\mu;y)+G(0,0;x)G(-\mu;y))-\frac{4}{9y^2}(8x^2+4xy-10x^2y-4y^2-5xy^2\\
&-4y^3)G(0,-\mu;y)+\frac{4(48x^2+44xy-15x^2y+13y^2-10xy^2-5y^3)}{9y^2}G(0;x)G(-\mu;y)\Big]\\
&+\frac{2(x-4)x(24x+16y-10xy+3y^2)}{9y^2\sqrt{x(4-x)}}G(\mu,0;x)-\frac{1}{9y^2}(288x^2+288xy-46x^2y\\
&+144y^2-52xy^2-17y^3)G(-\mu,-\mu;y)-(2x^2+2xy+y^2)\Big(\frac{4}{y}G(-\mu,-4,-\mu;y)\\
&+\frac{1}{15}G(0;y)+\frac{2(5y-12)}{9y^2}G(0,0;x)\Big)-\frac{2(4x^2+2xy+y^2)}{3y}G(-\mu,0,-\mu;y)\\
&-\frac{2}{3}(2x+y)(G(\mu,\mu,0;x)+G(0;x)G(-\mu,-\mu;y))-\frac{2}{27y^2}(432x^2+432xy\\
&-112x^2y+156y^2-136xy^2-65y^3)G(0;x)+\frac{2(4x^2+6xy+3y^2)}{3y}G(0,-\mu,-\mu;y)\\
&+\frac{2}{405y^2}(16176x^2+16896xy-3004x^2y+4488y^2-3004xy^2-1082y^3-1080x^2\zeta(2)\\
&-1080xy\zeta(2)+450x^2y\zeta(2)-540y^2\zeta(2)+450xy^2\zeta(2)+225y^3\zeta(2))\,, \qquad (186)
\end{aligned}
$$

$$
B_3^{(2l,-2)} = \frac{8x^2(5y-12)}{9y^2}-\frac{8x^2(y-2)(y+4)}{3y^2\sqrt{y(y+4)}}G(-\mu;y)\,, \qquad (187)
$$

$$
\begin{aligned}
B_3^{(2l,-1)} &= \frac{4(204x^2-36xy-13x^2y-36y^2+15xy^2+15y^3)}{27y^2}+\frac{4x^2(5y-12)}{9y^2}G(0;x)\\
&+\frac{8x^2}{3y}G(-\mu,-\mu;y)-\frac{y+4}{\sqrt{y(y+4)}}\Big[\frac{4}{9y^2}(34x^2-6xy-2x^2y-6y^2+3xy^2\\
&+3y^3)G(-\mu;y)+\frac{4x^2(y-2)}{3y^2}(3G(-4,-\mu;y)+G(0;x)G(-\mu;y))\Big]\,, \qquad (188)
\end{aligned}
$$

$$
\begin{aligned}
B_3^{(2l,0)} &= -\frac{2(x-4)x^3(y-2)(y+4)}{3y^2\sqrt{y(y+4)}\sqrt{x(4-x)}}G(\mu,0;x)G(-x-\mu;y)\\
&-\frac{y+4}{\sqrt{y(y+4)}}\Big[\frac{2x^2(y-2)}{3y^2}(G(-x,0,-\mu;y)-6G(-\mu,-\mu,-\mu;y))\\
&-\frac{1}{135y^2}(1736x^2-1020xy-82x^2y-1020y^2+60xy^2-9x^2y^2+60y^3-180x^2\zeta(2)\\
&+90x^2y\zeta(2))G(-\mu;y)+\frac{2}{3y^2}(34x^2-6xy-2x^2y-6y^2+3xy^2+3y^3)G(-4,-\mu;y)\\
&-\frac{2x^2(y-2)}{3y^2}(G(0;x)G(-x,-\mu;y)-G(0;x)G(0,-\mu;y)-3G(0;x)G(-4,-\mu;y)\\
&-9G(-4,-4,-\mu;y)+G(0,0,-\mu;y)-G(0,0;x)G(-\mu;y))\\
&+\frac{4x^2(5y-4)}{9y^2}G(0,-\mu;y)+\frac{2(14x^2-2xy-4x^2y-2y^2+xy^2+y^3)}{3y^2}G(0;x)G(-\mu;y)\Big]
\end{aligned}
$$

$$-\frac{2(x-4)x(12x-4y-5xy)}{9y^2\sqrt{x(4-x)}}G(\mu,0;x)-\frac{2}{405y^2}(4488x^2-2340xy-1082x^2y$$
$$-3060y^2+195xy^2+195y^3-540x^2\zeta(2)+225x^2y\zeta(2))+\frac{1}{9y^2}(144x^2-11x^2y$$
$$+12xy^2+12y^3)G(-\mu,-\mu;y)+\frac{4x^2}{3y}(3G(-\mu,-4,-\mu;y)+G(-\mu,0,-\mu;y)$$
$$-G(0,-\mu,-\mu;y))+\frac{2(180x^2-12xy-41x^2y-36y^2+15xy^2+15y^3)}{27y^2}G(0;x)$$
$$+\frac{x^2}{15}G(0;y)+\frac{2x^2(5y-12)}{9y^2}G(0,0;x)\,. \tag{189}$$

C Expansions of the Cross Section

The non-logarithmic part of the second order correction in Eq. (9) can be written as follows

$$\delta_0^{(2)}=-2\left[1+\ln\left(\frac{1-\xi}{\xi}\right)\right]\ln\left(\frac{4\omega^2}{s}\right)+Q_f^2N_c\left(\frac{\xi}{1-\xi+\xi^2}\right)^2 f(\rho,\xi)\,, \tag{190}$$

where the first term is determined by the soft emission and $f(\rho,\xi)$ is a function of two dimensionless variables: $\rho=m_f^2/s$ and $\xi=-t/s$. The small-mass expansion of the function $f(\rho,\xi)$ ($\rho=m_f^2/s$, $\xi=-t/s$) is of the following form

$$f(\rho,\xi)=\sum_{n=0}^{\infty}\rho^n f_n(\rho,\xi)\,, \tag{191}$$

where $f_n(\rho,\xi)$ depend on ρ only logarithmically. For the leading term we obtain

$$f_0(\rho,\xi)=\frac{(\xi^2-\xi+1)^2}{\xi^2}\left\{\frac{1}{9}\ln^3(\rho)+\ln^2(\rho)\left[\frac{1}{3}\ln(1-\xi)+\frac{19}{18}-\frac{1}{3}\ln(\xi)\right]\right.$$
$$\left.+\ln(\rho)\left[\frac{191}{27}+\frac{8}{3}\mathrm{Li}_2(\xi)\right]+\frac{40}{9}\mathrm{Li}_2(\xi)+\frac{1165}{81}\right\}-\ln(\rho)\Bigg[$$
$$+\frac{32\xi^4-46\xi^3+33\xi^2+8\xi-4}{6\xi^2}\zeta(2)-\frac{(\xi^2-\xi+1)(4\xi^2-7\xi+4)}{6\xi^2}\ln(1-\xi)^2$$
$$-\frac{20\xi^4-31\xi^3+60\xi^2-31\xi+20}{18\xi^2}\ln(1-\xi)+\frac{20\xi^4-67\xi^3+141\xi^2-112\xi+74}{18\xi^2}\ln(\xi)$$
$$+\frac{8\xi^4-\xi^3-15\xi^2+17\xi-4}{12\xi^2}\ln(\xi)^2-\frac{(2\xi-1)(4\xi^3-3\xi^2+4)}{6\xi^2}\ln(\xi)\ln(1-\xi)\Bigg]$$
$$+\frac{(2\xi-1)(\xi^2-\xi+1)}{3\xi}\zeta(3)-\frac{(\xi-1)^2(\xi^2-\xi+1)}{9\xi^2}\ln^3(1-\xi)$$
$$-\frac{196\xi^4-311\xi^3+258\xi^2+13\xi-38}{18\xi^2}\zeta(2)-\frac{2(2\xi^4-9\xi^3+16\xi^2-11\xi+4)}{3\xi^2}\ln(1-\xi)\zeta(2)$$
$$+\frac{12\xi^4-20\xi^3-\xi^2+24\xi-4}{6\xi^2}\ln(\xi)\zeta(2)+\frac{2(1-\xi^2)(\xi^2-\xi+1)}{3\xi^2}\ln(1-\xi)\mathrm{Li}_2(\xi)$$

$$
\begin{aligned}
&+\frac{7\,(16\xi^4-23\xi^3+48\xi^2-23\xi+16)}{54\xi^2}\ln(1-\xi)+\frac{20\xi^4-58\xi^3+81\xi^2-58\xi+20}{18\xi^2}\ln^2(1-\xi)\\
&-\frac{4\xi^3-6\xi^2+7\xi-4}{12\xi}\ln(\xi)\ln^2(1-\xi)+\frac{40\xi^4-50\xi^3+9\xi^2+37\xi-20}{18\xi^2}\ln(\xi)\ln(1-\xi)\\
&-\frac{\xi^4-3\xi^3+4\xi^2-\xi+1}{3\xi^2}\ln^2(\xi)\ln(1-\xi)+\frac{4\xi^4-2\xi^3-22\xi^2+31\xi-4}{36\xi^2}\ln^3(\xi)\\
&-\frac{20\xi^4+8\xi^3-84\xi^2+92\xi-55}{18\xi^2}\ln^2(\xi)-\frac{(\xi^2-\xi+1)(2\xi^2-7\xi+12)}{3\xi^2}\ln(\xi)\mathrm{Li}_2(\xi)\\
&-\frac{112\xi^4-449\xi^3+1011\xi^2-836\xi+562}{54\xi^2}\ln(\xi)\\
&+\frac{2(1-\xi^2)\,(\xi^2-\xi+1)}{3\xi^2}\mathrm{Li}_3(1-\xi)+\frac{(\xi^2-\xi+1)\,(2\xi^2-3\xi+4)}{3\xi^2}\mathrm{Li}_3(\xi)\\
&-\left(Q_f^2-1\right)\frac{(1-\xi+\xi^2)}{\xi^2}\left[(1-\xi+\xi^2)\left(\frac{5}{12}-2\zeta(3)+\frac{1}{2}\ln(\rho)\right)-\frac{2-\xi}{4}\ln(\xi)\right], \qquad (192)
\end{aligned}
$$

in agreement with the result of Refs. [26,44]. We observe that the functions f_i depend on the charge of heavy fermion Q_f through the contribution of the two-loop irreducible self-energy diagrams, which are proportional to Q_f^4, while all the other graphs that we consider in the present work are proportional to Q_f^2. The next-to-leading term is new and reads

$$
\begin{aligned}
f_1(\rho,\xi) \;=\;& \frac{2(\xi-1)\,(\xi^2-\xi+1)\,(2\xi^2+\xi+2)}{\xi^3}[\ln^2(\rho)+4\mathrm{Li}_2(\xi)+12]+\frac{\ln(\rho)}{\xi^3}\Big\{(\xi-1)(2\xi^4-5\xi^3\\
&+5\xi^2-5\xi+2)+2(\xi^2-\xi+1)[\left(4-2\xi+\xi^2-2\xi^3\right)\ln(\xi)+(\xi-1)(2+\xi\\
&+2\xi^2)\ln(1-\xi)]\Big\}-\frac{\zeta(2)}{\xi^3}(40\xi^5-54\xi^4+50\xi^3-17\xi^2-12\xi+8)+\frac{(\xi-1)}{2\xi^3}\Big[2(12\xi^4\\
&-5\xi^3+13\xi^2-5\xi+12)+(8-6\xi+9\xi^2-6\xi^3+8\xi^4)\ln(1-\xi)\Big]\ln(1-\xi)\\
&-\frac{1}{2\xi^3}\Big[2(12\xi^5-21\xi^4+26\xi^3-26\xi^2+21\xi-14)-2(4-6\xi-\xi^2+8\xi^3-10\xi^4\\
&+8\xi^5)\ln(1-\xi)+(8-15\xi+12\xi^2-\xi^3-7\xi^4+8\xi^5)\ln(\xi)\Big]\ln(\xi)\\
&+\left(Q_f^2-1\right)\frac{3}{\xi^3}\Big[(2-3\xi+4\xi^2-4\xi^3+3\xi^4-2\xi^5)\ln(\rho)\\
&-\left(2-3\xi+3\xi^2-\xi^3\right)\ln(\xi)\Big]. \qquad (193)
\end{aligned}
$$

The expansion in the large-mass limit takes the form

$$
f(\rho,\xi)=\sum_{n=0}^{\infty}\rho^{-n}\bar{f}_n(\rho,\xi)\,, \qquad (194)
$$

where the leading $n=0$ term vanishes because of the renormalization condition and $\bar{f}_n(\rho,x)$ depend on ρ only logarithmically. For the next-to-leading term we obtain

$$
\bar{f}_1(\rho,\xi) \;=\; \frac{955\xi^3-3926\xi^2+3926\xi-955}{1350\xi}-\frac{12\xi^3-19\xi^2+14\xi-6}{10\xi}\zeta(2)+\frac{3\xi^3+\xi^2-\xi-3}{30\xi}\ln(1-\xi)
$$

$$
\begin{aligned}
&+\frac{2\xi^3-5\xi^2+5\xi-2}{20\xi}\ln^2(1-\xi)+\frac{5\xi^3-22\xi^2+22\xi-5}{30\xi}\ln(\rho)\\
&-\frac{20\xi^3-78\xi^2+93\xi-58}{90\xi}\ln(\xi)+\ln(1-\xi)\frac{12\xi^3-19\xi^2+14\xi-6}{30\xi}\ln\xi\\
&+\frac{1}{60}\left(-6\xi^2+\xi+4\right)\ln^2(\xi)+\frac{4\left(\xi^3-2\xi^2+2\xi-1\right)}{5\xi}\mathrm{Li}_2(\xi)\\
&-\left(Q_f^2-1\right)\frac{41(\xi^3-2\xi^2+2\xi-1)}{54\xi}\,. \qquad (195)
\end{aligned}
$$

Finally, the next-to-next-to-leading order in the $s \ll m_f^2$ expansion reads

$$
\begin{aligned}
\bar{f}_2(\rho,\xi) \;=\; & -\frac{177763\xi^4-405359\xi^3+676194\xi^2-405359\xi+177763}{2116800\xi}\\
&+\frac{3\left(4\xi^4-17\xi^3+16\xi^2-12\xi+2\right)}{280\xi}\zeta(2)+\frac{2\xi^4+15\xi^3+6\xi^2+15\xi+2}{840\xi}\ln(1-\xi)\\
&-\frac{(\xi^2-4\xi+1)\left(2\xi^2-3\xi+2\right)}{560\xi}\ln^2(1-\xi)-\frac{53\xi^4-141\xi^3+222\xi^2-141\xi+53}{1680\xi}\ln(\rho)\\
&+\frac{33\xi^4-139\xi^3+213\xi^2-212\xi+52}{1680\xi}\ln(\xi)-\frac{4\xi^4-17\xi^3+16\xi^2-12\xi+2}{280\xi}\ln(\xi)\ln(1-\xi)\\
&+\frac{1}{560}\left(2\xi^3-4\xi^2-2\xi+1\right)\ln(\xi)^2-\frac{(\xi^2-4\xi+1)\left(\xi^2-\xi+1\right)}{35\xi}\mathrm{Li}_2(\xi)\\
&+\left(Q_f^2-1\right)\frac{449\left(1-5\xi+6\xi^2-5\xi^3+\xi^4\right)}{10800\xi}\,. \qquad (196)
\end{aligned}
$$

References

[1] H. J. Bhabha, Proc. Roy. Soc. Lond. A **154** (1936) 195.

[2] S. Jadach *et al.*, "Event Generators for Bhabha Scattering," arXiv:hep-ph/9602393.
G. Montagna, O. Nicrosini and F. Piccinini, Riv. Nuovo Cim. **21N9** (1998) 1 [arXiv:hep-ph/9802302].

[3] K. Mönig, *Bhabha scattering at the ILC*, Bhabha Mini-Workshop, Karlsruhe University, April 21-22, 2005.

[4] A. Denig, *Bhabha scattering at DAΦNE: the KLOE luminosity measurement*, Bhabha Mini-Workshop, Karlsruhe University, April 21-22, 2005.

[5] C. M. Carloni Calame, C. Lunardini, G. Montagna, O. Nicrosini and F. Piccinini, Nucl. Phys. B **584** (2000) 459 [arXiv:hep-ph/0003268].

[6] N. Toomi, J. Fujimoto, S. Kawabata, Y. Kurihara and T. Watanabe, Phys. Lett. B **429** (1998) 162.

[7] J. A. Aguilar-Saavedra *et al.* [ECFA/DESY LC Physics Working Group], arXiv:hep-ph/0106315.

[8] G. Abbiendi *et al.* [OPAL Collaboration], Eur. Phys. J. C **14** (2000) 373.
R. Barate *et al.* [ALEPH Collaboration], Eur. Phys. J. C **14** (2000) 1.

[9] A. Stahl, LC-DET-2005-004

[10] A. Aloisio *et al.* [KLOE Collaboration], Phys. Lett. B **606** (2005) 12.

[11] S. Eidelman [CMD-2 and SND Collaborations], PoS **HEP2005** (2006) 114.

[12] S. Jadach, W. Placzek, E. Richter-Was, B. F. L. Ward and Z. Was, Comput. Phys. Commun. **102** (1997) 229.

[13] C. M. Carloni Calame, C. Lunardini, G. Montagna, O. Nicrosini and F. Piccinini, Nucl. Phys. B **584** (2000) 459.
C. M. Carloni Calame, G. Montagna, O. Nicrosini and F. Piccinini, Nucl. Phys. Proc. Suppl. **131** (2004) 48.

[14] F. A. Berends and R. Kleiss, Nucl. Phys. B **228** (1983) 537.
F. A. Berends, R. Kleiss and W. Hollik, Nucl. Phys. B **304** (1988) 712.

[15] S. Jadach, W. Placzek and B. F. L. Ward, Phys. Lett. B **390** (1997) 298.
W. Placzek, S. Jadach, M. Melles, B. F. L. Ward and S. A. Yost, arXiv:hep-ph/9903381.

[16] A. B. Arbuzov, G. V. Fedotovich, E. A. Kuraev, N. P. Merenkov, V. D. Rushai and L. Trentadue, JHEP **9710** (1997) 001.

[17] M. Consoli, Nucl. Phys. B **160** (1979) 208.
M. Bohm, A. Denner and W. Hollik, Nucl. Phys. B **304** (1988) 687.
F. A. Berends and R. Kleiss, Nucl. Phys. B **228** (1983) 537.
M. Caffo, R. Gatto and E. Remiddi, Nucl. Phys. B **252** (1985) 378.

[18] G. Faldt and P. Osland, Nucl. Phys. B **413** (1994) 64 [arXiv:hep-ph/9304301]; Nucl. Phys. B **413** (1994) 16 [Erratum-ibid. B **419** (1994) 404] [arXiv:hep-ph/9304212].
A. B. Arbuzov, E. A. Kuraev and B. G. Shaikhatdenov, Mod. Phys. Lett. A **13** (1998) 2305 [arXiv:hep-ph/9806215].
A. B. Arbuzov, E. A. Kuraev, N. P. Merenkov and L. Trentadue, Nucl. Phys. B **474** (1996) 271.

[19] V. S. Fadin, E. A. Kuraev, L. Trentadue, L. N. Lipatov and N. P. Merenkov, Phys. Atom. Nucl. **56** (1993) 1537 [Yad. Fiz. **56N11** (1993) 145].

[20] A. B. Arbuzov, E. A. Kuraev, N. P. Merenkov and L. Trentadue, Phys. Atom. Nucl. **60** (1997) 591 [Yad. Fiz. **60N4** (1997) 673].

[21] S. Jadach, M. Melles, B.F.L. Ward, and S.A. Yost, Phys. Lett. B **450** (1999) 262.

[22] Z. Bern, L. Dixon, and A. Ghinculov, Phys. Rev. D **63** (2001) 053007 [arXiv:hep-ph/0010075].

[23] E. W. N. Glover, J. B. Tausk and J. J. Van der Bij, Phys. Lett. B **516** (2001) 33 [arXiv:hep-ph/0106052].

[24] A. A. Penin, Phys. Rev. Lett. **95** (2005) 010408 [arXiv:hep-ph/0501120]; Nucl. Phys. B **734** (2006) 185 [arXiv:hep-ph/0508127].

[25] R. Bonciani and A. Ferroglia, Phys. Rev. D **72** (2005) 056004 [arXiv:hep-ph/0507047].

[26] T. Becher and K. Melnikov, JHEP **0706** (2007) 084 [arXiv:0704.3582 [hep-ph]].

[27] A. Mitov and S. Moch, JHEP **0705** (2007) 001 [arXiv:hep-ph/0612149].

[28] V. A. Smirnov, Phys. Lett. B **524** (2002) 129 [arXiv:hep-ph/0111160].
G. Heinrich and V. A. Smirnov, Phys. Lett. B **598** (2004) 55 [arXiv:hep-ph/0406053].

[29] R. Bonciani, P. Mastrolia and E. Remiddi, Nucl. Phys. B **661** (2003) 289 [Erratum-ibid. B **702** (2004) 359] [arXiv:hep-ph/0301170].

[30] R. Bonciani, P. Mastrolia and E. Remiddi, Nucl. Phys. B **690** (2004) 138 [arXiv:hep-ph/0311145].

[31] A. I. Davydychev and M. Y. Kalmykov, Nucl. Phys. B **699** (2004) 3 [arXiv:hep-th/0303162].

[32] R. Bonciani, A. Ferroglia, P. Mastrolia, E. Remiddi and J. J. van der Bij, Nucl. Phys. B **681** (2004) 261 [Erratum-ibid. B **702** (2004) 364] [arXiv:hep-ph/0310333].

[33] M. Czakon, J. Gluza and T. Riemann, Phys. Rev. D **71** (2005) 073009 [arXiv:hep-ph/0412164].

[34] R. Bonciani, P. Mastrolia and E. Remiddi, Nucl. Phys. B **676** (2004) 399 [arXiv:hep-ph/0307295].

[35] R. Bonciani, A. Ferroglia, P. Mastrolia, E. Remiddi and J. J. van der Bij, Nucl. Phys. B **701** (2004) 121 [arXiv:hep-ph/0405275].

[36] R. Bonciani, A. Ferroglia, P. Mastrolia, E. Remiddi and J. J. van der Bij, Nucl. Phys. B **716** (2005) 280 [arXiv:hep-ph/0411321].

[37] S. Laporta and E. Remiddi, Phys. Lett. B **379** (1996) 283. [arXiv:hep-ph/9602417].
S. Laporta, Int. J. Mod. Phys. A **15** (2000) 5087. [arXiv:hep-ph/0102033].
C. Anastasiou and A. Lazopoulos, JHEP **0407** (2004) 046 [arXiv:hep-ph/0404258].
T. Gehrmann and E. Remiddi, Nucl. Phys. B **580** (2000) 485. [arXiv:hep-ph/9912329].

[38] F. V. Tkachov, Phys. Lett. B **100** (1981) 65.
G. Chetyrkin and F. V. Tkachov, Nucl. Phys. B **192** (1981) 159.

[39] A. V. Kotikov, Phys. Lett. B **254** (1991) 158; Phys. Lett. B **259** (1991) 314; Phys. Lett. B **267** (1991) 123.
E. Remiddi, Nuovo Cim. A **110** (1997) 1435. [arXiv:hep-th/9711188].
M. Caffo, H. Czyz, S. Laporta and E. Remiddi, Acta Phys. Polon. B **29** (1998) 2627; [arXiv:hep-th/9807119]; Nuovo Cim. A **111** (1998) 365. [arXiv:hep-th/9805118].
M. Argeri and P. Mastrolia, Int. J. Mod. Phys. A **22** (2007) 4375 [arXiv:0707.4037 [hep-ph]].

[40] A .B. Goncharov, Math. Res. Lett. 5 (1998), 497-516;
D. J. Broadhurst, Eur. Phys. J. C **8** (1999) 311, [arXiv:hep-th/9803091];
E. Remiddi and J. A. M. Vermaseren, Int. J. Mod. Phys. A **15** (2000) 725 [arXiv:hep-ph/9905237].

[41] T. Gehrmann and E. Remiddi, Comput. Phys. Commun. **141** (2001) 296 [arXiv:hep-ph/0107173]; Comput. Phys. Commun. **144** (2002) 200 [arXiv:hep-ph/0111255].

[42] D. Maître, Comput. Phys. Commun. **174** (2006) 222 [arXiv:hep-ph/0507152]; arXiv:hep-ph/0703052.

[43] J. Vollinga and S. Weinzierl, Comput. Phys. Commun. **167** (2005) 177 [arXiv:hep-ph/0410259].
S. Weinzierl, arXiv:0705.0900 [hep-ph].

[44] S. Actis, M. Czakon, J. Gluza and T. Riemann, Nucl. Phys. B **786** (2007) 26 [arXiv:0704.2400 [hep-ph]].

[45] M. Czakon, J. Gluza and T. Riemann, Nucl. Phys. B **751** (2006) 1 [arXiv:hep-ph/0604101].

[46] R. Bonciani, A. Ferroglia and A. A. Penin, arXiv:0710.4775 [hep-ph].

[47] S. Actis, M. Czakon, J. Gluza and T. Riemann, arXiv:0711.3847 [hep-ph].

[48] T. Kinoshita, J. Math. Phys. **3** (1962) 650.
T. D. Lee and M. Nauenberg, Phys. Rev. **133** (1964) B1549.

[49] D. R. Yennie, S. C. Frautschi and H. Suura, Annals Phys. **13** (1961) 379.

[50] V. A. Smirnov, *Applied Asymptotic Expansions in Momenta and Masses* (Springer-Verlag, Heidelberg, 2001).

[51] J. Frenkel and J. C. Taylor, Nucl. Phys. B **116** (1976) 185.

[52] J. Fleischer, A. V. Kotikov and O. L. Veretin, Nucl. Phys. B **547** (1999) 343 [arXiv:hep-ph/9808242].
U. Aglietti and R. Bonciani, Nucl. Phys. B **668** (2003) 3 [arXiv:hep-ph/0304028].

[53] U. Aglietti and R. Bonciani, Nucl. Phys. B **698** (2004) 277 [arXiv:hep-ph/0401193].

[54] D. Y. Bardin and G. Passarino, *The standard model in the making: Precision study of the electroweak interactions*, Oxford, UK: Clarendon (1999) 685 p.

[55] B. A. Kniehl, M. Krawczyk, J. H. Kuhn, and R. G. Stuart, Phys. Lett. B **209** (1988) 337.

[56] S. Groote, J. G. Korner and A. A. Pivovarov, Eur. Phys. J. C **24** (2002) 393 [arXiv:hep-ph/0111206].

[57] H. Czyz, A. Grzelinska, J. H. Kuhn and G. Rodrigo, Eur. Phys. J. C **33** (2004) 333 [arXiv:hep-ph/0308312].

[58] J. H. Kuhn, A. A. Penin and V. A. Smirnov, Eur. Phys. J. C **17** (2000) 97 [arXiv:hep-ph/9912503]; Nucl. Phys. Proc. Suppl. **89** (2000) 94 [arXiv:hep-ph/0005301].
J. H. Kuhn, S. Moch, A. A. Penin and V. A. Smirnov, Nucl. Phys. B **616** (2001) 286 [Erratum-ibid. B **648** (2003) 455] [arXiv:hep-ph/0106298].
B. Feucht, J. H. Kuhn, A. A. Penin and V. A. Smirnov, Phys. Rev. Lett. **93** (2004) 101802 [arXiv:hep-ph/0404082].
B. Jantzen, J. H. Kuhn, A. A. Penin and V. A. Smirnov, Phys. Rev. D **72** (2005) 051301 [Erratum-ibid. D **74** (2006) 019901] [arXiv:hep-ph/0504111]; Nucl. Phys. B **731** (2005) 188 [Erratum-ibid. B **752** (2006) 327] [arXiv:hep-ph/0509157].

[59] `hfbhabha.txt`, file included in the arXiv submission.

[60] J.A.M. Vermaseren, Symbolic Manipulation with `FORM`, Version 2, CAN, Amsterdam, 1991; "New features of FORM" [arXiv:math-ph/0010025].

[61] T. Huber and D. Maitre, Comput. Phys. Commun. **175** (2006) 122 [arXiv:hep-ph/0507094]. arXiv:0708.2443 [hep-ph].

[62] S. Friot, D. Greynat and E. De Rafael, Phys. Lett. B **628** (2005) 73 [arXiv:hep-ph/0505038].

[63] Leonard Lewin, *Polylogarithms and Associated Functions*, Elsevier Science (1981) 359 p.